Thermometry of flow fields using a two-color ratiometric PLIF technique

by

Seth M. Heronemus

B.S., Kansas State University, 2016

A THESIS

submitted in partial fulfillment of the requirements for the degree

MASTER OF SCIENCE

Department of Mechanical and Nuclear Engineering
College of Engineering

KANSAS STATE UNIVERSITY
Manhattan, Kansas

2018

Approved by:

Major Professor
Dr. Steve Eckels

Copyright

Abstract

In this thesis, a two-color ratiometric planar laser-induced fluorescence (PLIF) technique for the measurement of temperature fields in liquids is described. The method uses the temperature sensitive rhodamine B and temperature insensitive rhodamine 110 fluorescent dyes. The ratio of the fluorescent emission intensity of these two dyes is inversely proportional to temperature and is independent of laser intensity variation in the flow field. Because the emission spectra of these two dyes overlap, a correction was developed to disentangle the two signals. In addition, the absorption spectra of rhodamine B and rhodamine 110 and emission spectrum of rhodamine 110 overlap, leading to the self-attenuation of the rhodamine 110 signal by the dye solution. A correction with respect to path length was developed for self-attenuation. This thesis presents the calibration process for a PLIF thermometry system and visualization of temperature gradients in a glass water tank with motion induced by large temperature gradients. A step-by-step procedure of the final calibration process is also presented.

Table of Contents

List of Figures

List of Tables

Acknowledgements

I would like to acknowledge and extend my gratitude to Dr. Steve Eckels for the support and guidance I have received in the pursuit of my degree and research interests. I would also like to thank the Matt Campbell and Kaitlin Bachle with the Institute for Environmental Research for their day to day support of my research. The other graduate students at IER have been very generous with their time and advice when I asked for it and I am very grateful to them. Garrett Mann was very helpful to me as I began my research and I am very grateful for all of the advice he gave me. I'd also like to thank the rest of my committee, Dr. Terry Beck and Julia Keen, for their time and encouragement. I am very grateful for my loving wife and family as well as my friends and all their encouragement and patience.

Chapter 1 - Introduction

The study of fluid flows requires accurate means of measuring fluid properties such as the pressure, temperature, density, and velocity. In many applications, such as heat exchangers, the movement of energy and momentum is of particular interest. It is vital to have the ability to take accurate measurements throughout the flow volume. Temperature measurements are used to study the heat transfer processes that occur within these flows and with their surroundings. Many sensors and measurement techniques have been developed and utilized for this purpose. The technique of planar laser induced fluorescence (PLIF) has been used in numerous applications to give accurate full field temperature measurements. This research expands on previous work done to develop and calibrate PLIF thermometry techniques in liquids.

Thermocouples and resistance temperature detectors are simple thermometry devices used in a variety of applications. Thermocouples consist of two wires of different material joined at a junction at one end. The junction experiences a temperature change at the point of measurement that produces a voltage. The voltage can then be converted and read as the measured temperature change. This phenomenon is known as the Seebeck Effect which states that a temperature difference at two dissimilar conductors connected in a circuit produces a voltage difference (Caltech, 2018). Thermocouples can measure temperature over a large temperature range.

Resistance temperature detectors (RTD) are another means to measure temperature locally. RTDs consist of a resistor connected to an electric circuit that measures resistance. The device operates on the principle that a conductor's resistance increases with increased temperature (National Instruments, 2016). RTDs are calibrated to read the correct temperature based on the resistance in the circuit.

Thermocouples and RTDs are very accurate tools for measuring local temperature. However, they can only take measurements at a single point in the flow. They also must be placed within the flow to measure temperature and so alter the flow mechanics. As a result, they are better suited for applications with very large flow structures or in cases where the precise flow characteristics are not important.

There are many instances where the information provided by temperature probes is insufficient to study fluid flows. Sometimes it is necessary to know the temperature distribution throughout the flow. In addition, for small scale or complex fluid flows to be studied accurately, non-invasive temperature measurements are extremely important. Puxuan et al. (2018) used particle image velocimetry (PIV) to measure full field velocity and validate numerical simulations for different inlet conditions in turbulent flows. Full field temperature measurements would allow validation of the temperature distributions calculated by these numerical models.

There are many methods for achieving full field temperature measurements. One technique is to coat a surface with a luminescent substance whose phosphorescence characteristics change with temperature. Yi, Kim, and Kim (2014) studied temperature distributions on a phosphor coated aluminum plate that was heated and then cooled with an air nozzle. Euler et al. (2014) measured the temperature of a bluff body surface as it cooled after being subjected to a methane/air flame. The bluff body was coated with a phosphor that was excited by a 266nm laser. They were able to obtain a resolution of 290μm x 133μm. Phosphor coated surfaces can be used for measurements of many different types of systems to take full field temperature measurements at the interface between a flow and a surface. However, for measurements within the flow, other techniques must be examined.

Thermochromic liquid crystals (TLCs) can provide full field thermometry both at solid, liquid interfaces and within the flow. The crystals dissolve in a liquid flow and are illuminated by white light. They give off a different color of light proportionate to their temperature. TLCs have been used to study the flow in a differentially heated cavity. Measurements taken with TLCs showed good agreement with the temperature distribution and velocity profile computed with numerical simulations (Kowalewski, 2001). TLCs were also used to help find heat transfer coefficients while trying to determine the best hole arrangement for an impingement and effusion cooling system for gas turbines. The crystals used had a temperature band of only 1°C over which they changed color. The TLCs were shown to have an accuracy of ±0.13°C based on the standard deviation of measurements (Andreini et al., 2018). Their effectiveness can be limited by the range of temperature being studied. The band over which they change color is narrow, generally in the range of 0.5°C to 20°C (Kowalewski, 2001). This makes them impractical to use in applications where large temperature ranges are being studied. TLCs also need white light illumination, which generally has a limited intensity range, making high resolution measurements difficult (Vogt and Stephan, 2012).

Planar laser induced fluorescence is an extremely versatile measurement technique that has been used in a wide variety of applications. The technique can be adapted to measure a number of different fluid properties, including velocity, temperature, concentration, and pressure. In this technique, fluorescent dyes are dissolved in the flow and excited with a laser. The laser light is optically formed into a sheet to measure properties along a plane. The intensity of the fluorescence emissions from these excited dyes is dependent on temperature, concentration, and pressure. The intensity of light given off is measured by a light sensor. The measured intensities can then be converted to give the value of the measured property. PLIF was even recently used to measure pH

at different points in a flow. Lacassagne et al. (2018) were able to measure pH in a volume of neutral fluid that was impinged by an acidic jet. If concentration, pressure, and pH are held constant, then temperature can be measured. The accuracy of measurements with PLIF techniques is dependent on holding these and all other variables constant in the experimental setup. If any property cannot be held constant, then the physics of fluorescence and the measurement system need to be well understood and appropriate corrections for changes can be determined. Researchers use a variety of methods and experimental setups to calibrate measurement systems and hold variables constant.

PLIF techniques can be classified by the number of dyes they use and by the number of different spectral bands being observed and recorded during measurements. Temperature measurements have been made using single-color/single-dye techniques. Xu et al. (2010) measured water temperature using a wide portion of the emission spectrum of rhodamine B (RHB) dye and the intensity at all temperatures was normalized by the intensity measured at 293K. This method was able to reach a global uncertainty of ±1K. Using volume illumination LIF in a microchannel, Chamarthy et al. (2010) normalized the intensity of the fluorescence signal from RHB at different temperatures to the intensity at a reference temperature and obtained pixel to pixel uncertainty of 1.25°C and area averaged uncertainty of 0.6°C. Using this technique, they were able to measure temperature distributions in a microchannel heat sink.

Single color techniques have some limitations. They do not account for fluctuations in incident light intensity across the measurement field or shot to shot laser intensity variation. To account for variations in laser intensity, a two-color/two-dye method can be employed where simultaneous images are taken measuring the intensity of a temperature insensitive and sensitive dye. Kim and Kihm (2001) used RHB and rhodamine 110 (RH110) as the temperature sensitive

and insensitive dyes to perform this technique. They were able to obtain temperature measurements with an uncertainty of ±1.45°C with a 95% confidence interval and a spatial resolution of 300µm by 200µm. In another study, Hishida and Sakakibara (2000) used RHB and RH110 to study a three-dimensional temperature field from thermal convection on a horizontal uniformly heated surface. The laser sheet moved horizontally, and shots were taken at 60hz to obtain the three-dimensional measurements. West (2012) used a two dye PLIF technique to measure natural convection from a cartridge heater in a water tank. The temperature sensitive dye was Europium (III) thenoyltrifluoroacetoneate and the temperature insensitive dye was Coumarin 500.

A two-color ratiometric technique can also be implemented using one dye. The method is almost the same as the two-dye technique. Two different spectral bands are still chosen to be observed. The difference is that the bands are chosen from the emission spectrum of one dye. The bands must have different temperature sensitivities, though. These systems typically have less temperature sensitivity than two dye systems (Bruchhausen et al., 2005). Examples of applications of this technique include Abram et al. (2016), who explored thermographic phosphor particles for temperature measurement of a buoyant thermal plume and achieved a precision of 2-3°C using a two-color technique. Bruchhausen et al. (2005) used two different spectral bands of RHB for their measurement system. They used their calibrated system to measure the temperature distribution of a heated jet injected into an ambient temperature fluid. They compared their results for both an instantaneous temperature measurement and a measurement averaged over 100 images. PLIF is a versatile and accurate means of measuring both instantaneous and time averaged temperature profiles non-intrusively in a variety of different systems.

This thesis describes the process of calibrating a two-color ratiometric thermometry system and taking measurements of temperature gradients. The work will expand on previous work with PLIF systems to develop corrections for fluorescent signal attenuation due to path length and signal overlap of the temperature sensitive and insensitive dyes. First, the process of fluorescence will be defined and explained in more detail. The governing equation for fluorescence will be described and the benefit of using a ratio of intensity signals will be shown. The dye selection process will be described. Complications due to overlapping absorption and emission spectra will be discussed. Next, the equipment used in the measurement setup will be described. Corrections to the fluorescence equation for signal overlap and self-attenuation will be determined. The calibration process used to develop this measurement system will be described. The image processing procedure used for all intensity images taken with this measurement system will be discussed. A calibration curve for temperature vs intensity ratio was produced. To further improve the accuracy of temperature measurements, an image normalization process is introduced. The calibration curve is adapted to incorporate normalization. From the normalized calibration curve, an equation for temperature is determined. This equation is used to produce temperature images. The resolution and uncertainty of the measurement system are discussed. The results of measuring a temperature gradient are shown. And finally, a finalized and detailed calibration procedure will be described.

Chapter 2 - Fluorescence Description and Dye Selection

In the two-color PLIF technique, laser light is used to excite fluorescent dyes and the intensity of the light produced by those dyes is measured. Fluorescence is the process by which a certain type of molecule, called a fluorophore, absorbs light and then emits light at a longer wavelength. The fluorescence process is comprised of three main stages (Davidson, M., et al., 2015). First, the molecule is excited from a ground state to an excited electronic state by absorbing an incident photon. This excited state is subdivided into several vibrational energy levels. During the first stage, the molecule is excited to a vibrational energy level above the first. Next, the molecule undergoes a non-radiative relaxation process down to its lowest vibrational energy level of the excited state (Scientific Volume Imaging). During the vibrational relaxation period, the molecule loses some of the incident energy to interactions with its molecular environment. Finally, the excited fluorophore will release its remaining excess energy and return to the ground state. A diagram of the fluorescence process is shown in Figure 1.

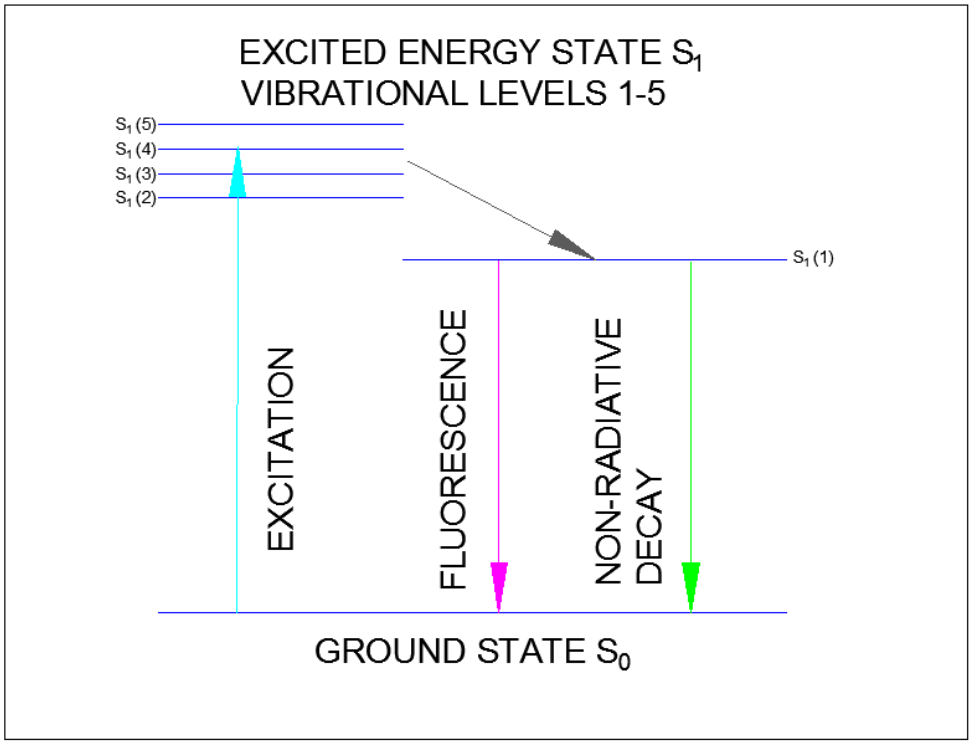

Figure 1 Diagram of the fluorescence process (Scientific Volume Imaging).

Excited molecules can release excess energy and return to the ground state in several different ways. The excited molecule can emit a photon of fluorescent light. This photon will have a longer wavelength than the absorbed photon, a phenomenon known as the Stokes shift (Davidson, M., et al., 2015). Another key property of fluorescence is that the fluorescence emission spectrum of a particular molecule is independent of the wavelength of the exciting light as long as the exciting light falls within the absorption spectrum of the dye (Thermo Fisher, 2018).

However, not all molecules that absorb a photon will use the emission of a photon to return to the ground state. Collisional quenching, fluorescence resonance energy transfer, and intersystem crossing are all non-radiative means for the fluorophore to return to the ground state (Thermo Fisher, 2018). The quantum efficiency of a fluorescent material is the ratio of photons that are emitted via fluorescent emission to the number of photons that are absorbed from the

incident light. The quantum efficiency is particularly important for this technique because for some dyes, the quantum efficiency can be temperature dependent (Amiri et al., 2014). Therefore, if all other equation parameters can be held constant, fluorescence can be used for temperature measurements.

The governing equation of fluorescence provides key insight into how to make accurate measurements of temperature using PLIF. The intensity of fluorescent light emitted by a molecule I_f is proportional to the incident exciting light I_0 (laser light intensity at the point of absorption), the concentration of the fluorescent dye C, the quantum efficiency of the dye Q, and the absorption coefficient of the dye ε (Yamaguchi et al., 2006). The fluorescence emission equation is given in Eq. 1.

$$I_f = I_0 \varepsilon C Q \tag{1}$$

For it to be possible to measure temperature accurately with fluorescence, all parameters of the fluorescence equation, except the quantum efficiency, must be held constant in the viewing window. While absorption coefficient and concentration can be assumed to remain constant throughout the field, I_0 will depend on the point in the field that the laser light is absorbed by the dye. The laser light intensity will decrease the further it travels through the medium according to Beer's Law (NMSU, 2006). In addition, spreading the laser light out into a sheet can cause non-uniform intensity. Finally, laser intensity can vary as much 6-7% from shot to shot (Bruchhausen et al., 2005). To account for varying incident light intensity, a ratio of fluorescent intensity signals can be used. The signals for the ratio can be captured by two cameras. One can capture light from a temperature sensitive dye and one from a temperature insensitive dye. With proper alignment, the cameras will be reading intensities of two different dyes from the same point in the field. The dyes at the same location will receive the same amount of incident light.

There are several important properties considered when choosing fluorescent dyes for an experimental setup. Both dyes needed to be soluble in water, which was the media in which measurements would be conducted. In addition, one of the dyes needed to have strong temperature dependent fluorescent intensity and one dye needed to be largely temperature insensitive. The temperature dependence of fluorescent molecules is generally small (Kim and Kihm, 2001). However, some dyes, such as RHB and Fluorescein 27, have strong temperature dependence based on their quantum efficiency. Finally, a 532nm laser was used as the source of incident light for the setup. Therefore, both dyes needed to be capable of absorbing and reemitting 532nm light. Rhodamine B and rhodamine 110 were found to be the dye combination that best fit these criteria. RHB has a temperature sensitivity close to 2.3%/K (Yamaguchi et al., 2006). In addition, both dyes have absorption spectra that include 532nm light and both are soluble in water.

The corresponding signal from each of these dyes is given as I_B and I_{110}, respectively. Forming a ratio of the intensity signals given by Eq. 1 for each dye with the temperature sensitive RHB in the numerator yields Eq. 2.

$$\frac{I_B}{I_{110}} = \frac{\varepsilon_B C_B Q_B}{\varepsilon_{110} C_{110} Q_{110}} \tag{2}$$

As discussed earlier, taking a ratio of intensities cancels I_0. In addition, the ratios of absorption coefficient and concentration are constant in the viewing field. Therefore, the ratio of RHB and RH110 is only dependent on quantum efficiency, which is temperature dependent for RHB.

Once the dyes were chosen, their spectral properties needed to be examined more closely. The interactions between the two dyes are important for determining accurate equations and corrections for the measured fluorescence intensity. Figure 2 shows the absorption and emission spectra of the two dyes.

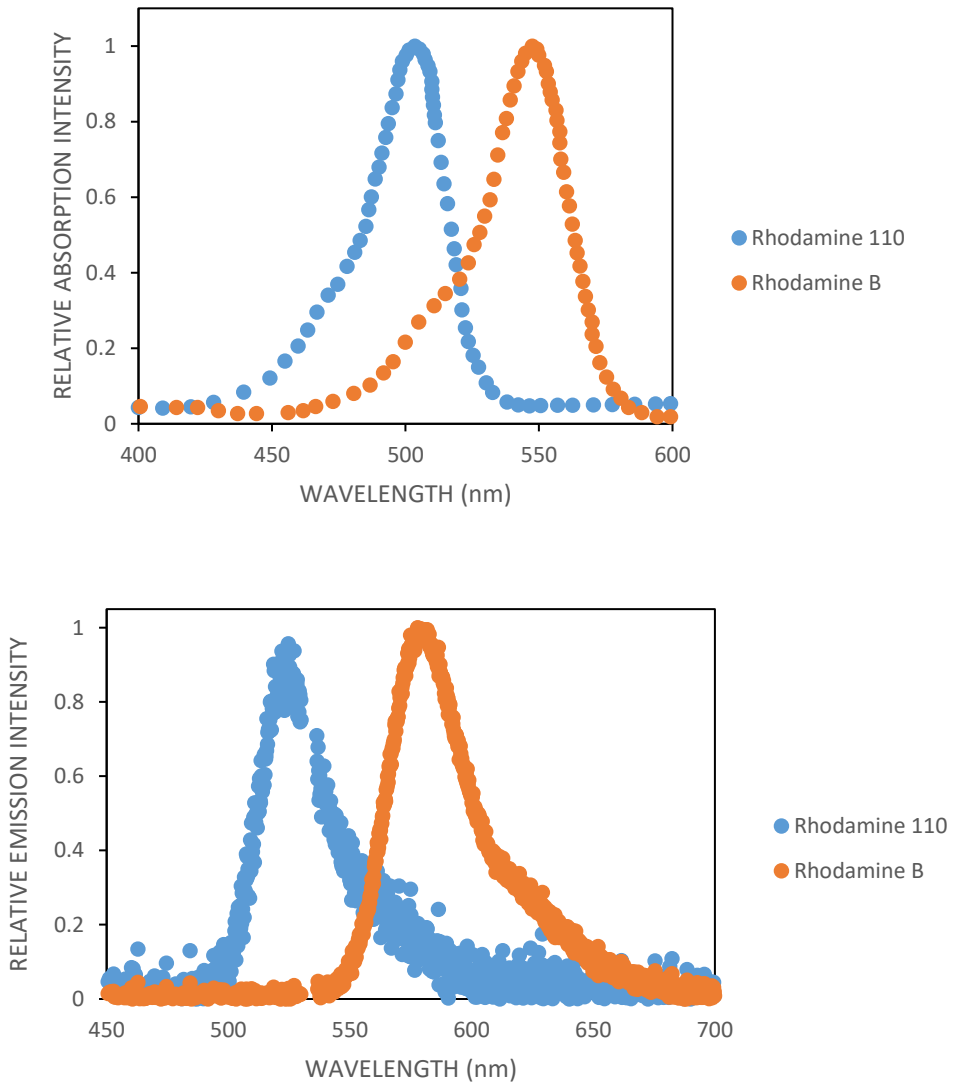

Figure 2 The absorption (top) and emission (bottom) spectra of RHB and RH110.

The spectra graphs reveal several issues that will need to be addressed. As the figure shows, the emission spectra of the two dyes cross one another. This will lead to the RHB signal having temperature insensitive RH110 signal mixed into the readings. In addition, the absorption spectra of both RHB and RH110 overlap the emission spectrum of RH110. This will lead to reabsorption of the RH110 signal by the solution and decrease the measured signal relative to what

the emitted intensity signal would have been. Further discussion of these spectral issues and the development of corrections for them are discussed in the Experimental Setup section of this thesis.

Chapter 3 - Experimental Setup

Originally, the experimental setup was situated so that the two cameras were facing each other. Each camera had its own lens and filter to isolate one of the two dye signals. The configuration was modeled after the one used by West (2012) for the development of temperature sensitive beads for thermometry and velocimetry. However, the setup had several issues that made it difficult to work with. Alignment of the two cameras was difficult. Each was placed on its own stand and so had to be adjusted to match the height and location of the other. Then the angle and tilt of each of the cameras had to be matched to ensure they had the same viewing window. Finally, the focal planes of the cameras had to be aligned and lined up with the laser sheet. In addition, the filters reflected the light that they didn't allow in and the opposing camera saw that light, giving inconsistent results. Having two camera lenses also meant that the system had more sources for error in the images. It was decided that a setup using one camera lens and a dichroic mirror to split the incoming signal would simplify camera alignment and eliminate the potential for reflected light interference.

The preferred measurement system consists of a 573nm dichroic mirror, two cameras, a shared 100mm camera lens, a 515nm bandpass filter and a 575nm longpass filter, and a mounting box that the two filter mounts and the shared camera lens attach to. The cameras are attached to their respective filter mounts. A photograph of the new measurement system is shown in Figure 3.

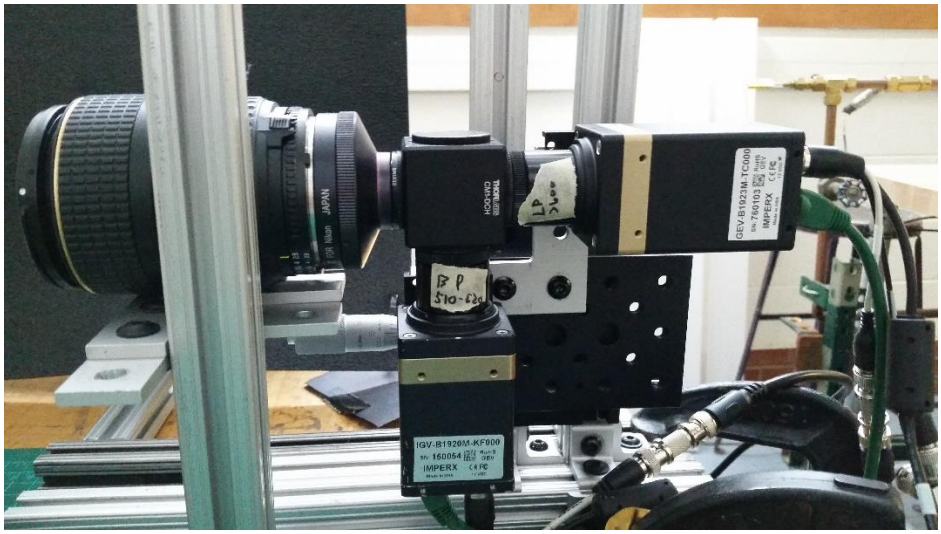

Figure 3 Shows a photograph of the measurement system. The dichroic mirror is mounted in the box in the center of the photograph.

The measurement system uses two charge-coupled device (CCD) cameras to record the fluorescence signal produced by the dissolved dyes. CCD cameras have a semiconductor sensor that records the number of photons that strike its surface at a given pixel location. An electrical charge is recorded that is proportionate to the number of photons and this electric charge is converted to a voltage (Mootz and Mathews, 2008). This voltage is then interpreted as a pixel intensity. The pixel intensities are then sent to the computer where the camera software Bobcat GEV Player interprets the signal, displays the images and can save the images in a chosen folder as .tif files. The cameras each have sensors of 1920 x 1080 pixels. The camera used for recording the RHB signal is designated as camera 1and the camera recording the RH110 signal is designated as camera 2.

The dichroic mirror is imperative for this setup because it allows the cameras to share a camera lens. A dichroic mirror is a device that allows some wavelengths of light to pass through it while reflecting others. The mirror needed to be chosen so that it directed 510-520nm wavelength light in one direction and all light greater than 575nm wavelength light in another

direction to separate the signals seen by the cameras with their respective filters. All dichroic mirrors have a transition region, wavelengths where the dichroic mirror is transitioning from reflecting wavelengths to transmitting them. The mirror for this measurement system, a 573nm dichroic mirror, was chosen with a steep cutoff to limit the region of the longpass filter that would be in the transition region. A graph of the transmission spectrum for the chosen dichroic mirror is shown in Figure 4.

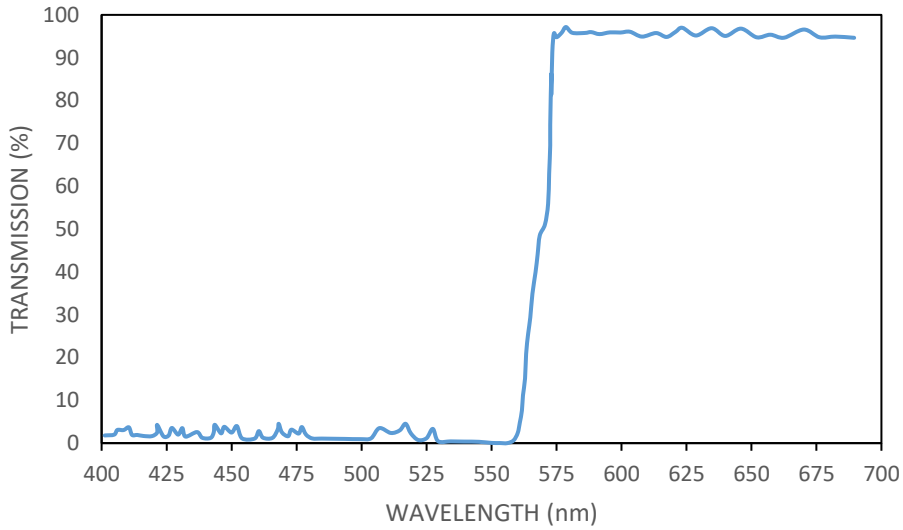

Figure 4 Graph of the light transmission percentage as a function of wavelength for the chosen dichroic mirror.

Filters needed to be selected for each camera to further isolate the signals from the two fluorescent dyes. A 575nm longpass filter was chosen for camera 1 to isolate the RHB signal. This wavelength was chosen to maximize the RHB signal seen by the camera while minimizing the RH110 signal let through by the filter. A 515nm bandpass filter was chosen for camera 2. This filter was chosen to be close to the maximum of the RH110 emission spectrum. The absorption and emission spectra of the two dyes along with the filter wavelength bands are shown in Figure 5.

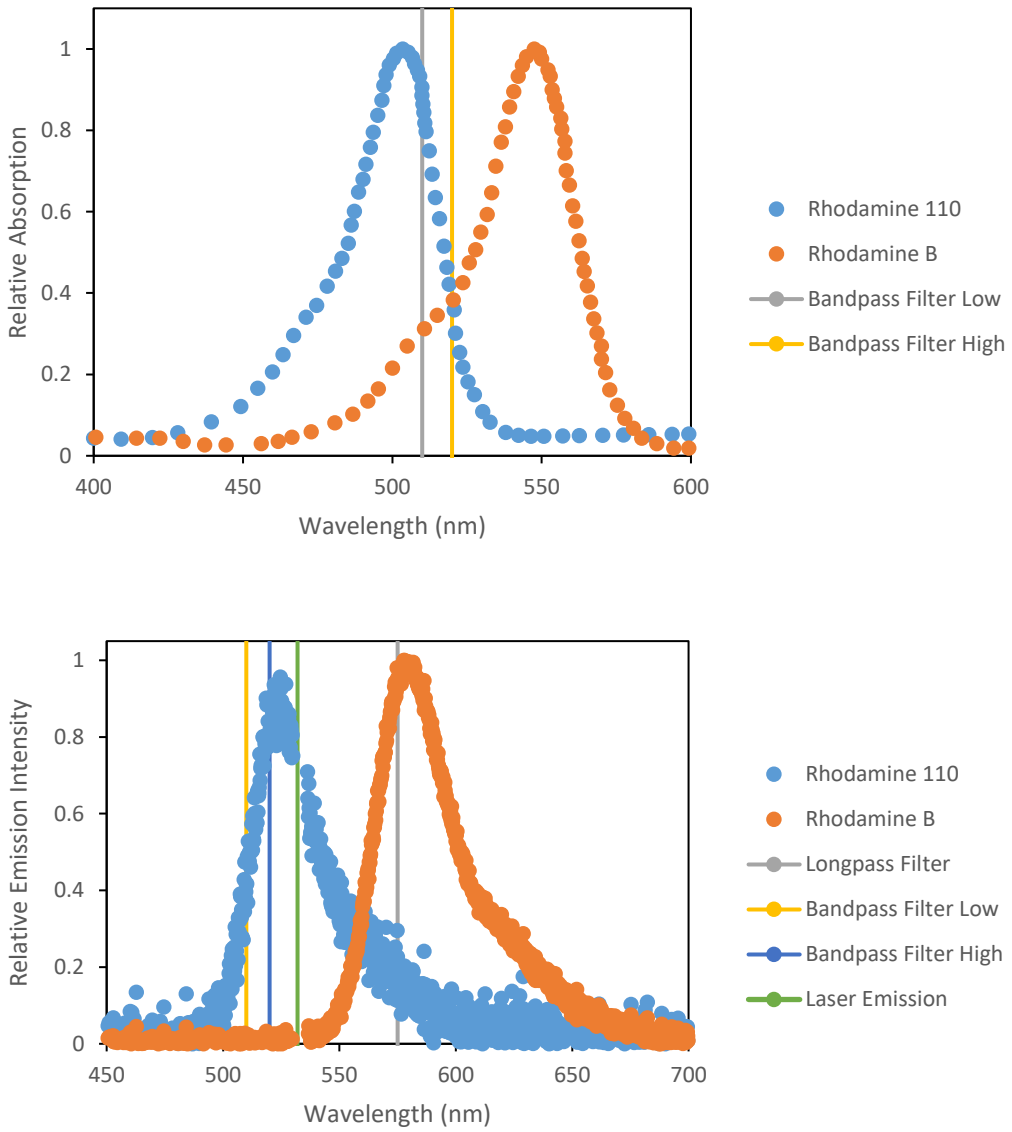

Figure 5 The absorption (top) and emission (bottom) spectra of RHB and RH110. Filter spectral bands and laser emission wavelengths are also given.

A photograph of the entire experimental setup is shown in Figure 6. It is comprised of a 532 nm laser, a tank with fluorescent dye dissolved in DI water, a function generator (not pictured), and the measurement system. The glass tank sits on a hotplate that is used to adjust the temperature of the solution and for creating temperature gradients for temperature measurements.

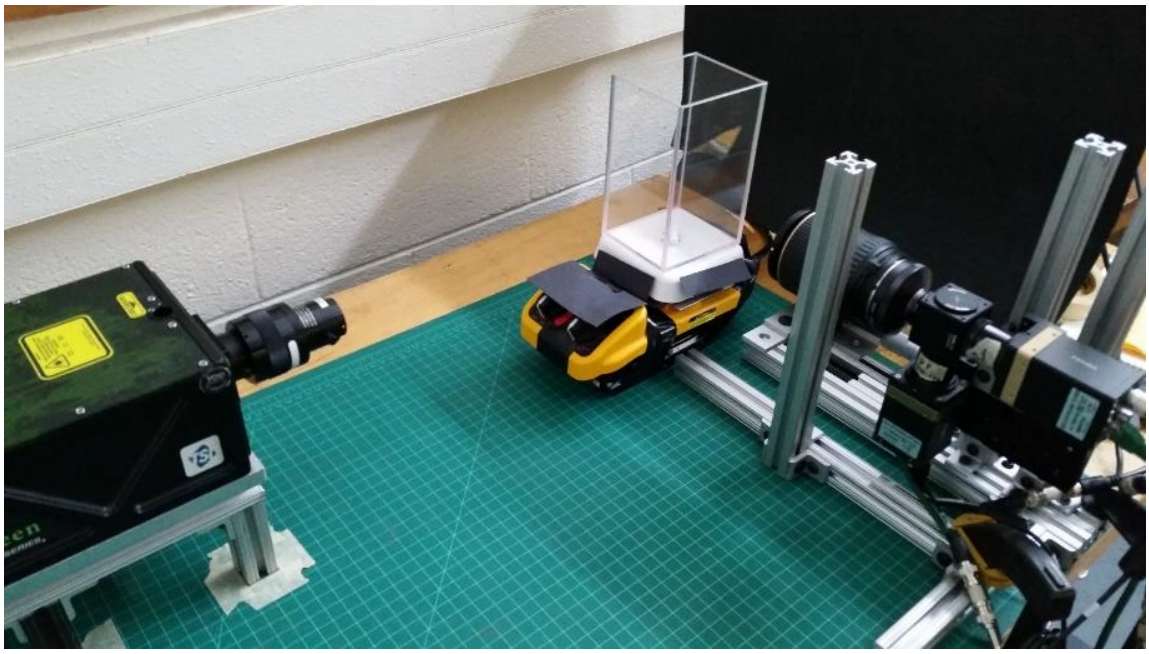

Figure 6 Photograph of the experimental setup.

For this experimental setup, it was important that all equipment maintain the same position throughout the experiment. First the positioning of the cameras was set, and the focal plane of the cameras was found. The extensions behind the camera lens of the dichroic mirror box and the filter housings and associated adapters made the exact location of the focal plane difficult to calculate. However, the location could be found by moving a target in front of the camera lens until the images taken of the target by the cameras came into focus. The target was also used to determine that the viewing window of the cameras is 2cm x 1.1cm. The laser was positioned so that the laser sheet was coplanar with the cameras' focal plane. Finally, the position of the tank relative to the laser plane needed to be known for the system calibration. To maintain proper positioning, a mat with one half-inch grid lines was used to mark specific locations for the laser, camera, and hotplate. Exact movement of the tank for the system calibration could be performed using the grid marks.

Another important consideration for the setup was to maintain constant concentration for the fluorescent dye solution. A stock solution of each dye was made with a concentration of 25mg/L. Each was made by combining 25mg of fluorescent dye powder with 950mL of distilled water and 50mL of methanol. Precise amounts of the stock solutions were measured using a volumetric pipet to make the dye solution. One liter of a solution of 0.125mg/L of RHB and 1mg/L of RH110 was created and used for calibration and temperature measurements. Different concentrations of RHB were considered, but the chosen concentration was shown to give the most consistent results. In addition, Zhang and Dong (2015) showed that within the temperature range of 20°C to 50°C the sensitivity to temperature of RHB is not dependent on concentration. Therefore, consistency of results was chosen as the most important criteria for choosing concentration.

The 532nm laser is formed into a sheet using a collimator and cylindrical lens. The collimator produces a beam of extremely uniform thickness. The cylindrical lens forms the laser light into a sheet. The purpose of the laser sheet is to view a two-dimensional cross section of the fluid. However, the laser sheet has a thickness of 1mm. The fluorescent signal measured by the cameras at each point is an integration of the signal over the entire thickness of the laser sheet. Therefore, all temperature measurements taken with this setup, at a given point in the viewing window, will be an average fluid temperature over that thickness. A summary of the optical components used in the experimental setup are shown in Table 1.

Table 1 Summary of optics used in used in the experimental setup.

Optical Component	Description	Manufacturer
Camera Lens	100mm lens 55mm diameter	Tokina
Bandpass Filter	515nm CWL, 10nm FWHM, 25mm Mounted Diameter	Edmund Optics
Longpass Filter	575nm 25mm Dia., High Performance Longpass Filter	Edmund Optics
Dichroic Mirror	573nm 25mmx36mm	Semrock
Collimator	Adjustable focal length of 300mm to 4000mm	TSI
Cylindrical Lens	25mm	TSI

The function generator is used to synchronize the image capture of the two cameras. The signal rate is set to a frequency of 5hz and sends a square wave signal to both cameras. The cameras are set to external trigger mode and upon receiving a signal from the function generator, begin their image capture sequence. One of the cameras is also set on pulse mode. Upon receiving the trigger signal, the camera sends out a delayed signal to one of the two laser lamps. The signal delay is timed so that the laser fires after the cameras' exposure time has started. This ensures that the entire fluorescence event will be captured by the measurement system.

Once the laser fires, some of the laser light is absorbed by the fluorescent dye. The light emitted by the dye is the total fluorescence I_f. Once the fluorescent signal from the dye leaves the tank, it travels a short distance through the intervening space and enters the camera lens. It contacts the 573nm dichroic mirror mounted behind the lens. The mirror is mounted at a 45-degree angle to the incident signal and allows the longer wavelength portion of the signal to pass through the mirror and pass through a 575nm longpass filter before reaching camera 1. The shorter wavelength portion of the signal is reflected by the mirror, passes through a 515nm bandpass filter and then is

recorded by camera 2. The image from camera 2 is flipped to undo the reversal caused by the mirror. Figure 7 shows a schematic view of the experimental setup.

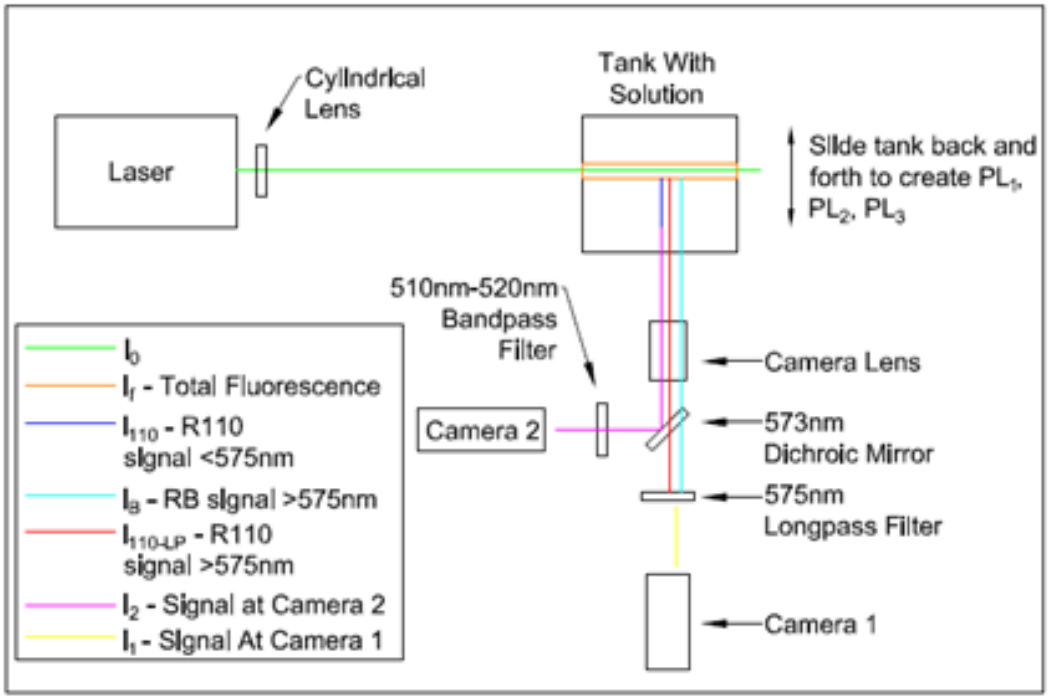

Figure 7 A schematic of the experimental setup. The various intensity signals as they travel through the setup are named and pictured.

Figure 7 also shows a schematic of the path taken by each portion of the dye signals as they travel through the experimental setup. It can be seen in the emission graph in Figure 5 and is shown schematically in Figure 7 that the longpass filter doesn't completely separate the dye signals. Camera 1 sees some signal from RHB, I_B, and some signal from RH110, $I_{110\text{-}LP}$ to give the total measured signal, I_1. To account for this in the fluorescence equation, a ratio of $I_{110\text{-}LP}$ and the signal seen by camera 2, I_2, needs to be determined. The ratio of the two R110 signal portions, M, is given as Eq. 3.

$$M = \frac{I_{110-LP}}{I_2} \tag{3}$$

The process of determining M will be described in the calibration section of this work. Once determined, this ratio can then be multiplied by the measured I_2 signal to subtract the $I_{110\text{-}LP}$ signal from I_1 for a given image. Eq. 2 is modified as shown in Eq. 4.

$$\frac{I_B}{I_{110}} = \frac{I_1 - M * I_2}{I_2} \tag{4}$$

Another consequence of the chosen dye combination is the attenuation of I_{110} by the mixed dye solution. Figure 5 shows that the absorption spectra of both dyes overlap the portion of the emission spectrum of RH110 seen by camera 2. As a result, a fraction of the I_{110} signal is reabsorbed by the dye in the solution. The longer the path length (PL) or the distance through the medium that the fluorescence emission travels to reach the camera, the lower the recorded I_2 signal, will be. According to Bruchhausen et al. (2005), the absorption is governed by Lambert's law, given in Eq. 5.

$$I_2 = I_{110} * e^{-\psi \mathrm{PL}} \tag{5}$$

In this case, I_2 is the signal out of the solution and seen by camera 2, I_{110} is the initial fluorescent emission, ψ is the extinction coefficient, and PL is the path length. A further description of dye PL is given in Figure 8 which shows a schematic of the dye signal passing through the mixed solution and out of the tank.

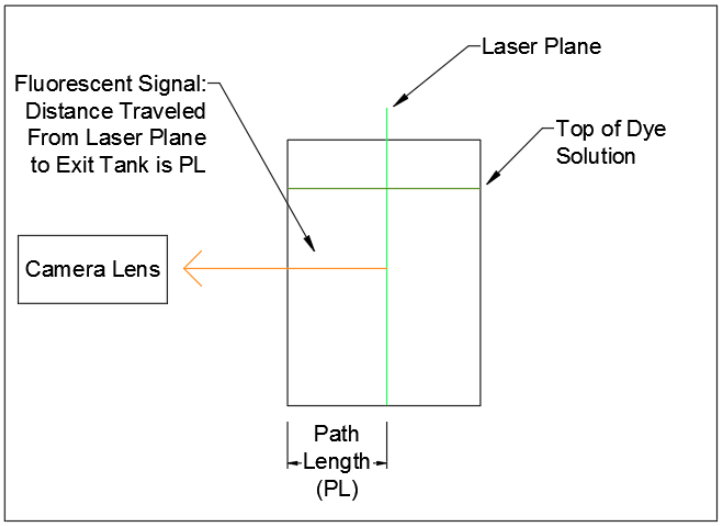

Figure 8 Schematic to define signal path length.

Solving Eq. 5 for I_{110} and inserting into the bottom of Eq. 4 yields an equation for the intensity ratio with corrections for path length and signal crossing, given as Eq. 6. Eq. 5 is only substituted into the bottom of Eq 4. because M is based on the uncorrected R110 signal, I_2.

$$\frac{I_B}{I_{110}} = \frac{I_1 - M * I_2}{I_2 * e^{\psi \mathrm{PL}}} \tag{6}$$

Determination of M required a calibration using a solution with only RH110 dye at the same concentration as in the two-dye solution which will be discussed later in this section. Determination of ψ will be discussed in the Results and Analysis section of this paper.

The next objective was to develop a calibration curve for the intensity ratio of RHB to RH110 and temperature. Images taken with both cameras (image sets) were recorded for five different temperatures. The solution was heated to the measurement temperatures using the hotplate and the temperature was monitored in the viewing window using three thermocouples. The thermocouples were placed so that the sensors were at the same height in the solution as the measurement window. The solution was heated slowly to each calibration temperature and measurements were taken once the temperature of the solution had stabilized to the desired

temperature according to the thermocouple measurements. Images were obtained at three different path lengths, 1in, 2in, and 3in, for each calibration temperature. The intensity ratio values at three different path lengths enabled ψ to be found to relate I_2 to I_{110} using Eq. 5. The path length for the fluorescence signals was changed by shifting the tank forward or backward (keeping the rest of the setup stationary) to change the position of the laser sheet relative to the front of the tank as shown in Figure 7. Thirty sets of images were taken for each combination of path length and temperature. Bruchhausen et al., (2005) used a similar calibration procedure to determine if path length affected their temperature measurements. In their case, a correction was not necessary because the intensity results for both spectral bands were the same regardless of path length.

In addition to path length, M needed to be determined so that signal crossing could be corrected. To do this, the same calibration setup was used except the solution in the tank only contained RH110. Thirty image sets were taken at five different path lengths to determine if the ratio was dependent on path length. The average intensity value for each image from camera 1 gives $I_{110\text{-}LP}$ values, and the average value from each camera 2 image gives I_2 values. M was found using Eq. 3 and plotted against path length as shown in Figure 9.

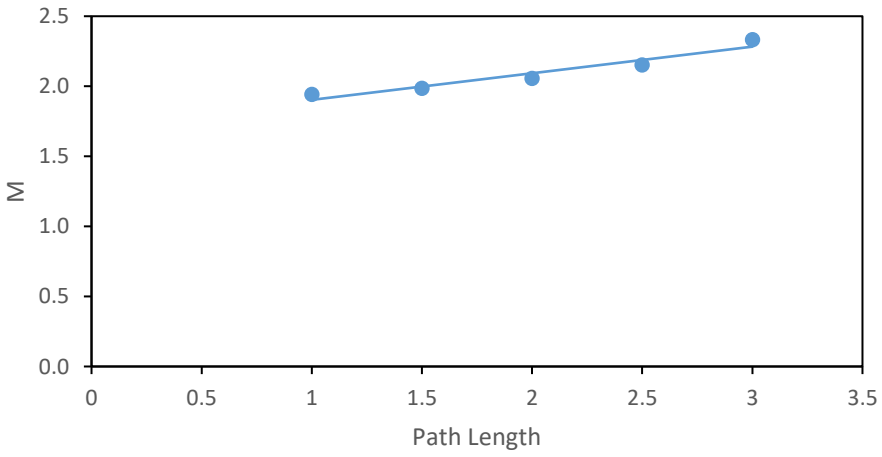

Figure 9 Plot of M vs path length.

Each dot on the graph consists of 30 M values found with 30 image sets. The plot shows that M varies linearly and decreases with a longer path length. A curve for the graph was found using a linear least squares method. The R squared value of the graph was found to be 0.93. Using the curve fit, M can be chosen to subtract the $I_{LP\text{-}110}$ signal from I_1 for temperature measurements.

Chapter 4 - Image Processing

Once the 15 calibration image sets were obtained, they were imported into MATLAB and processed one at a time. The code for image alignment, obtaining average image intensity values for calibration and calculating temperature values for image sets is given in Appendix A of this document.

MATLAB's image processing toolbox was used to read the .tif image files from each camera and store them in two three-dimensional arrays. Once imported, a background subtraction is applied to each image. Initially, a set of background images was taken each time an image set was taken. However, the calibration images were taken in a room with the lights off, the windows completely covered and with all instrument lights covered or facing away from the setup. As a result, it was found that the background images had almost no variation from one set of shots to another. The decision was made that one set of background shots could be used because of the lack of variation between background shots and the background intensity was so much smaller than the measurement intensities. The process for importing background images and subtracting from the analyzed image set is shown in both the Calculate Average Image Intensities and Determine Image Temperatures sections of Appendix A.

Camera alignment is very important for the two-color PLIF technique. It allows the variation in laser intensity throughout the measurement window to be cancelled out by the intensity ratio. Both cameras were manually aligned as closely as possible. To further refine the camera alignment, images of a target were taken using both cameras. The target used was a millimeter ruler which was also used to find the size of the viewing window. The alignment images were overlaid using MATLAB software. Figure 10 shows an image created by MATLAB of the overlay of an image from both cameras of the target.

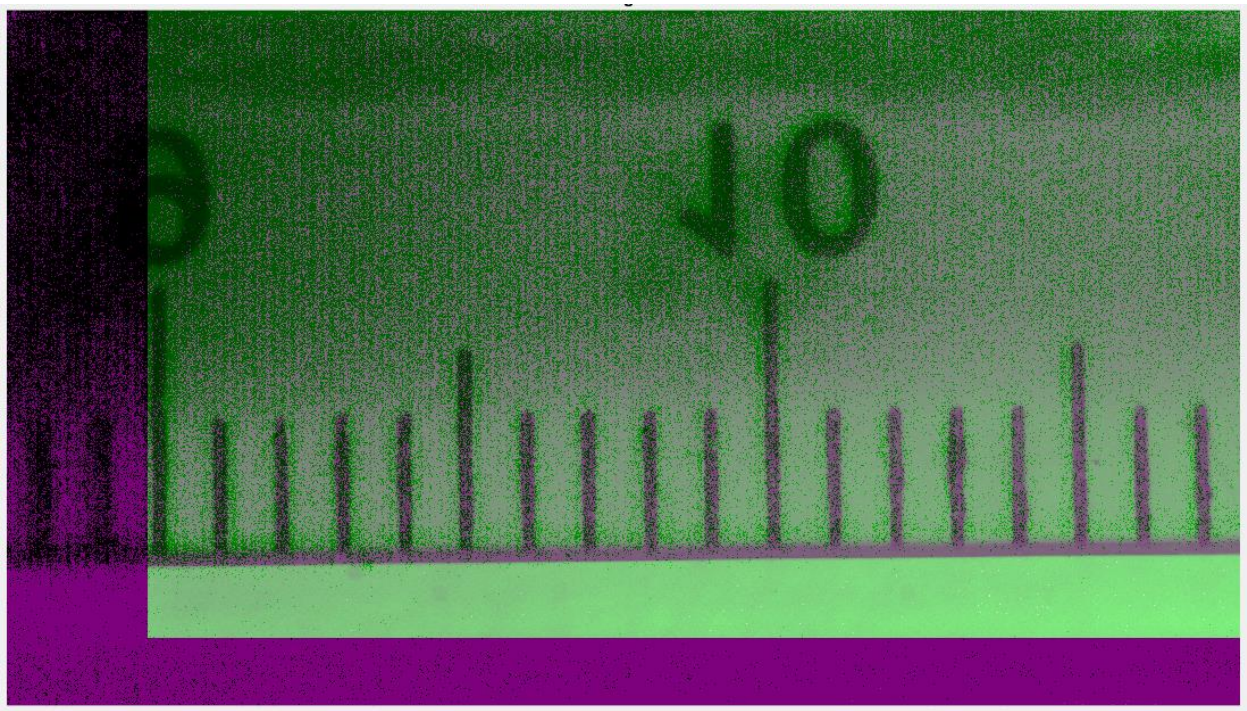

Figure 10 An overlay of an image of the target from both cameras created by MATLAB.

MATLAB's image translate function was used to shift one image to align as closely with the other as possible with a user input translation. Different combinations of horizontal and vertical shifts were applied until the closest alignment possible was found. No rotation was needed to create the alignment. The user input shift function was checked using the image register function which automatically aligns images by matching intensity patterns and found to give the same alignment. This shift was applied to all imported images and only the overlapping sections of the images were used. After the shift was applied, the images were 1820 x 890 pixels with a viewing window size of 1.9cm x 0.91cm. The Image Alignment section of Appendix A shows the MATLAB code used for this process.

When intensity maps of individual images were inspected, images from camera 2 showed vertical bands of alternating higher and lower intensity along the length of the images. The bands

can be seen in Figure 11, which shows an intensity plot of an image taken by camera 2 during the 30°C, 3in PL calibration measurement.

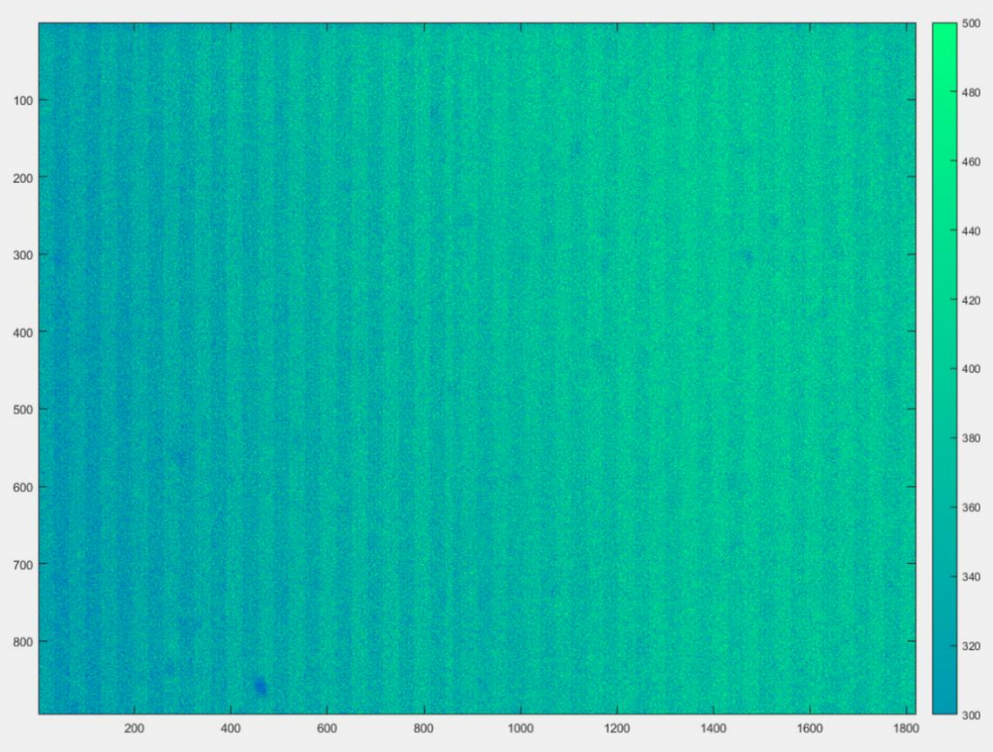

Figure 11 Camera 2 intensity plot showing vertical banding.

The bands are 30 pixels across. The intensity of the alternating bands was explored to determine if there was a repeating pattern that could be corrected or subtracted out. Table 2 shows the average intensity for the full height of the image for the first five bands. It was expected that a pattern of higher intensity and then lower intensity averages would be seen based on the scale of the intensity plot. However, as the data in the table shows, the average only increases slightly from the left to the right of the image.

Table 2 Average intensity within bands.

Pixel Range for Band	Average Intensity
1-30	314.87
31-60	315.56
61-90	316.47
91-120	319.51
121-150	321.38

Two different methods were attempted to suppress the banding pattern. One method was to divide a banded image by another in the same set. If the pattern was consistent from image to image, this method should divide out much of the pattern. The ratio image was then multiplied by the average intensity from the original image. The result is shown in Figure 12.

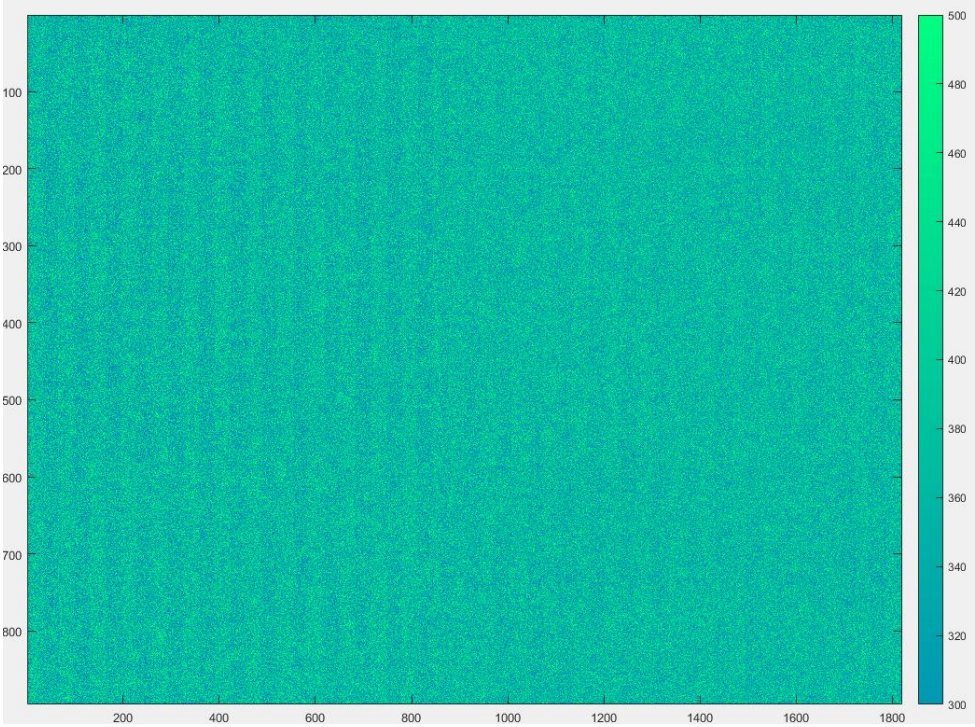

Figure 12 One banded image divided by another and multiplied by the average.

The figure shows that while there was some suppression of the banding, it is still clearly visible. The second solution was to take each pixel within the image and make its value the

average of the eight adjacent pixels and the original value to damp out the banding pattern. An image after this solution is applied is shown in Figure 13.

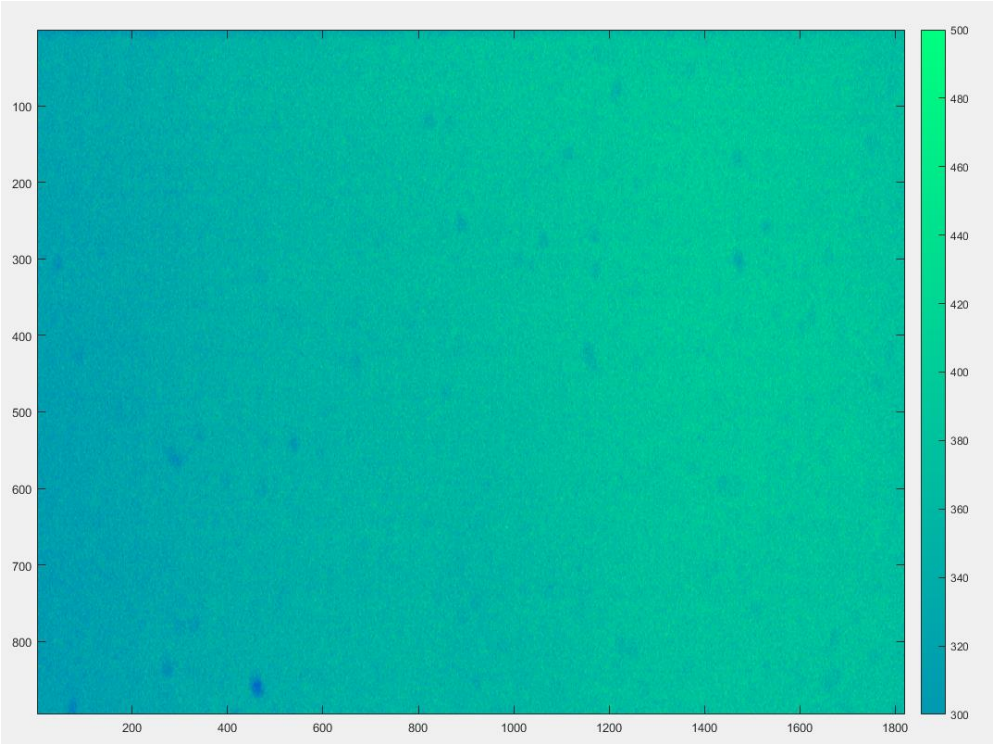

Figure 13 Camera 2 intensity plot after the block average correction.

Figure 13 shows that the block average correction eliminates the banding pattern. This solution preserves the overall intensity pattern within the image by applying a correction at a small local level. The reduction of intensity variation is shown by computing the average, standard deviation, high, and low intensity values for each of the camera 2 images in the 30°C, 3in PL calibration image set. These values were computed before and after the block averaging process was applied and the averages of those values are given in Table 3.

Table 3 Impact of the block average method on image intensity variation.

	Average Intensity	Standard Deviation of Intensity	Maximum Intensity	Minimum Intensity
Before Block Average	338	52	1601	0
After Block Average	338	26	559	129

As Table 3 shows, the maximum and minimum intensity values moved towards the mean. The standard deviation of the intensity within the images was cut in half. The average intensity within the images was unchanged. These results imply that the block average method was able to decrease image intensity variation while keeping the overall intensity within the image intact. This solution was applied to all camera 2 images. The code for implementing the block average method is shown in both the Calculate Average Image Intensities and Determine Image Temperatures sections of Appendix A. After alignment and banding corrections were applied, images were ready for analysis.

Chapter 5 - Results and Analysis

Once the image processing steps were determined, a calibration curve was created to relate temperature and corrected intensity ratio. The average intensity value of each image taken during the calibration process was computed. These values were calculated using the code shown in Calculate Average Image Intensities in Appendix A. The average intensity values were used as the I_1 and I_2 values in the equations for determining the calibration curve. These average intensities are plotted in Figure 14.

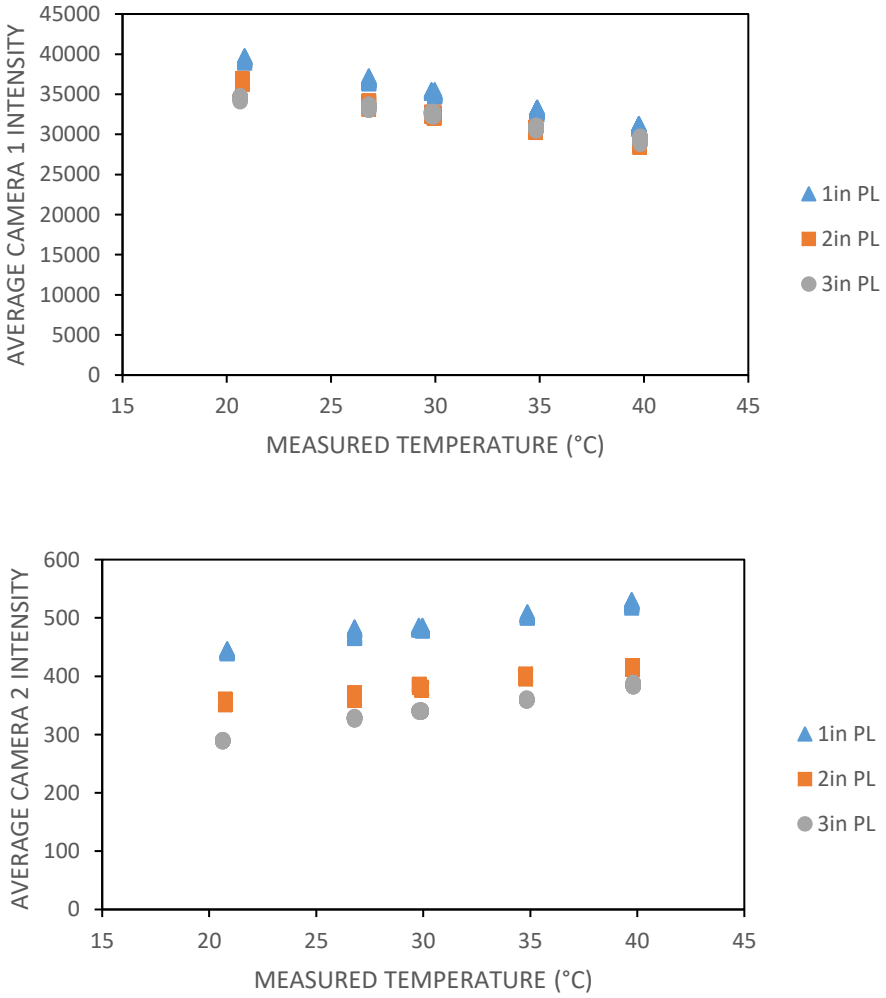

Figure 14 Plot of measured temperature vs camera 1 (top) and camera 2 (bottom) average intensities.

Each point on the graph is a cluster of 30 image intensity averages corresponding to the 30 image sets taken at each combination of temperature and path length. The graph of camera 2 intensities vs temperature clearly shows the need for a correction for path length. There are three distinct curves corresponding to the three different calibration path lengths. The graph also shows an increase in intensity with temperature for the camera 2 signal. This was unexpected since RH110 was chosen as the temperature insensitive dye. The variation with temperature is likely due to a temperature dependence of the self-absorption. As the temperature increases, less of the initial fluorescence signal is re-absorbed by the dye. The path length correction does not remove the induced temperature dependence of the camera 2 signal. However, this turns out to be beneficial. The intensity graphs show that the signals from the two cameras have reverse temperature dependencies. As a result, the system will have more temperature sensitivity than if the signal from camera 2 was temperature insensitive. This technique has been used before in the development of a PLIF system. Estrada-Perez et al. (2011) used Rhodamine B and Fluorescein 27, two temperature sensitive dyes, to develop a two-color thermometry method. Fluorescein has fluorescent intensity proportionate to temperature and RHB, as discussed, has intensity inversely proportionate to temperature. Using these two dyes, they were able to achieve increased temperature sensitivity over what is reported when only using one temperature sensitive dye.

Once the average intensities were determined for each image, the ratio of the corresponding I_1 and I_2 averages was determined for each of the combinations of path length and temperature. A plot of these values is given in Figure 15.

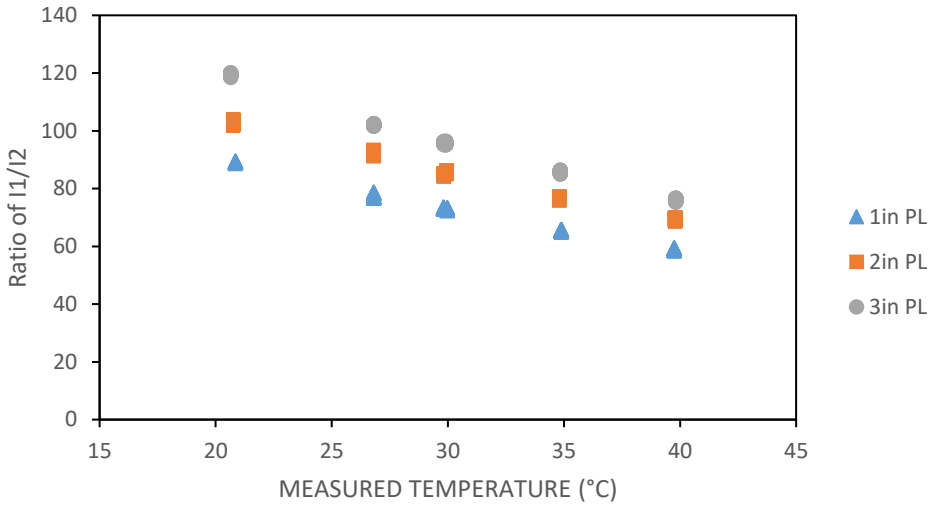

Figure 15 Plot of measured temperature vs I_1/I_2.

The figure shows that even after taking a ratio of the intensity values, there are still three distinct curves corresponding to the three different path lengths at which calibration data was taken.

Based on the plot of intensity ratio vs temperature shown in Figure 15, the relationship is linear. From Eq. 6, a linear calibration equation relating measured temperature to measured camera intensity is given in Eq. 7 where a, b, and ψ are unknowns that need to be found from the calibration data.

$$a + b * T = \frac{I_1 - M * I_2}{I_2 * e^{\psi \mathrm{PL}}} = R \tag{7}$$

For simplification, the corrected intensity ratio will be defined as R. An optimization program was used to solve for the unknowns with the goal of minimizing T_{error}. Eq. 8 gives the equation to determine $T_{calculated}$.

$$T_{calculated} = \frac{R - a}{b} \tag{8}$$

T_{error} is defined in Eq. 9 and is found by taking the absolute value of the difference between the calculated temperature based on Eq. 8 and the measured temperature for each image set. The goal of the solver was to find the minimum value for the average of T_{error}.

$$T_{error} = \overline{abs(T_{measured} - T_{calculated})} \tag{9}$$

The solver obtained a minimum average error between measured and calculated temperature of 0.62°C. The values for the variables were found to be 105.66, 1.443, and 0.1418, for a, b, and ψ respectively. Using these optimized values, a calibration curve was plotted using Eq. 7. The calibration curve is given in Figure 16.

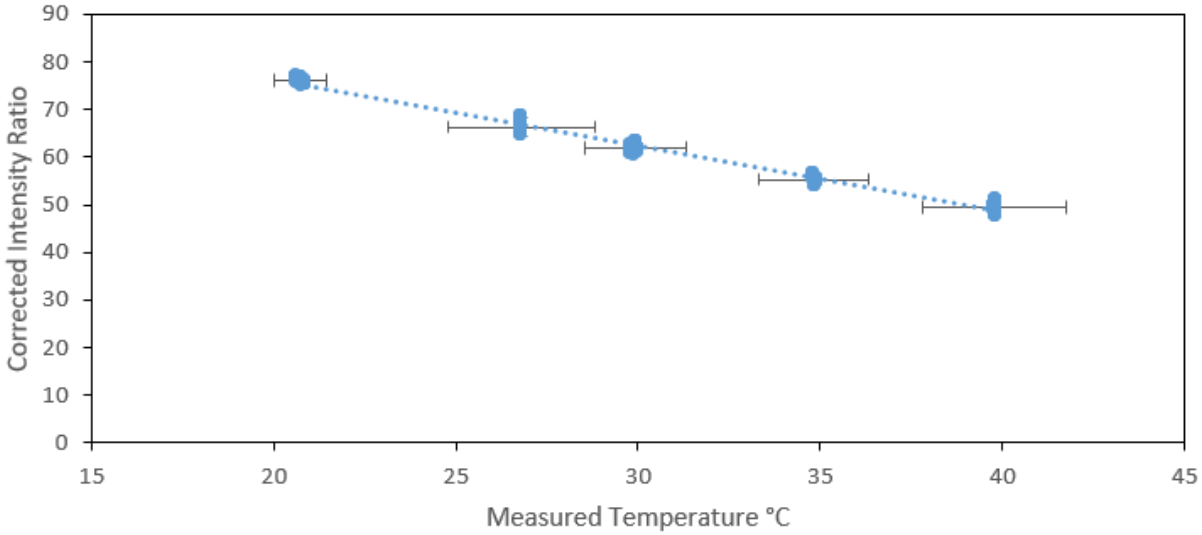

Figure 16 Plot of measured temperature vs corrected intensity ratio, R.

Error bars for the graph were found by determining the standard deviation of the calculated average temperature for the calibration images with respect to the measured temperature. The standard deviation for each measurement temperature was multiplied by 1.96 to give the 95% confidence interval for each measurement temperature. Error bars were then

plotted with length equal to the 95% confidence interval, $CI_{95\%}$. An equation for finding the length of the error bars for each measurement temperature is shown in Eq. 10.

$$CI_{95\%} = 1.96 * \sqrt{\frac{\sum(T_{measured} - T_{calculated})^2}{N - 1}} \tag{10}$$

Solving Eq. 7 for T gives an equation for temperature based on the corrected intensity ratio. The equation for temperature is given in Eq. 11.

$$T = \frac{R - a}{b} \tag{11}$$

Once the calibration curve was created, and an equation for temperature was found, temperature images could be produced by finding pixel by pixel corrected intensity ratios and applying the temperature equation at each pixel. A temperature image produced from one of the images taken during calibration with a measured temperature of 30°C and a PL of two inches is shown in Figure 17.

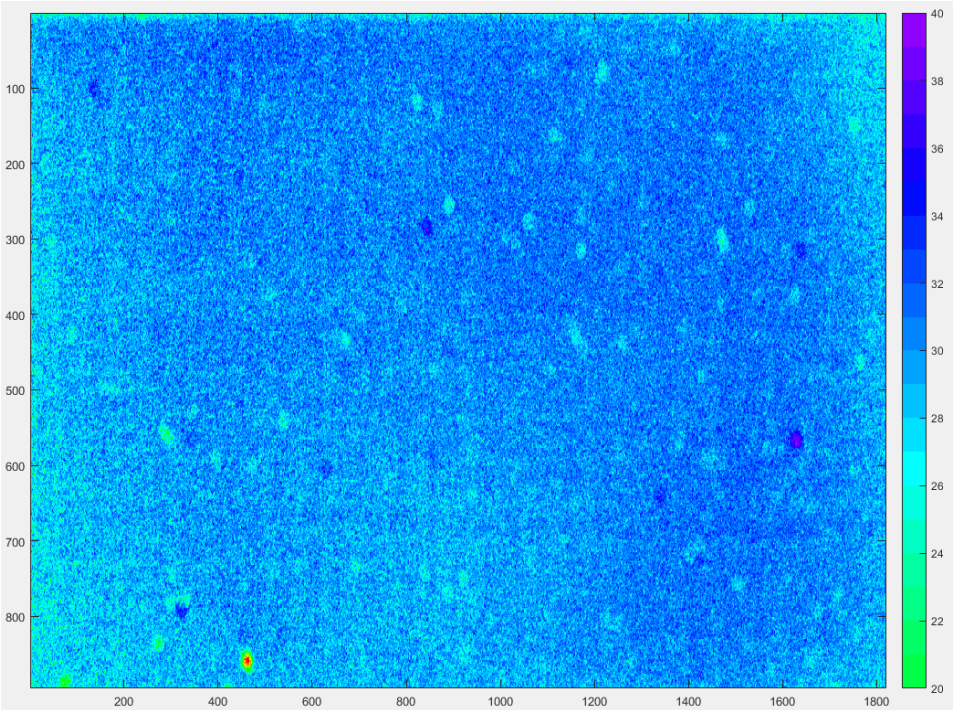

Figure 17 Temperature image at 30°C based on corrected calibration curve.

The figure shows that there is overall good agreement between the calculated temperatures and the measured temperature where the color scale corresponding to temperature in degrees Celcius is shown to the right of the image. However, the temperature image shows some optical features, large spots of high or low temperature, that were not removed by taking a ratio of the images from the two cameras. This could be due to features on the camera sensors or on the longpass/bandpass filters, which only one camera would see. To remove these features and obtain as accurate a temperature reading as possible, it was decided to normalize all camera images. Normalization is a common method for eliminating the effect of the detection system (Bruchhausen et al., 2005). Normalization is performed by obtaining a reference image at a known temperature and dividing all subsequent measurements by that reference image. For this system, since images from two different cameras need to be normalized, a normalization matrix, Φ, was created by finding the average corrected intensity ratio, R, at each pixel over the entire 20°C image set and taking the inverse at each pixel. The R matrix from each set of camera 1 and 2 images was multiplied by Φ to give the normalized intensity ratio Ω as shown in Eq. 12.

$$\Omega = R * \Phi \tag{12}$$

Before temperature images could be created using the normalized intensity ratio, a new calibration curve needed to be created. The same process was used to form the new calibration curve except Φ was added to Eq. 7 to give Eq. 13.

$$a + b * T = \Phi \frac{I_1 - M * I_2}{I_2 * e^{\psi \mathrm{PL}}} = \Omega \tag{13}$$

For the calibration curve, the variable Φ is an average of the values within the matrix. The far right-hand side of the equation, Ω, is now the normalized intensity ratio. Eq. 8 was also modified to use the normalized intensity ratio, as shown in Eq. 14.

$$T_{calculated} = \frac{\Omega - a}{b} \tag{14}$$

Solving the optimization equation again yields values of 1.3913, 0.019, and 0.1418 for a, b, and ψ and an identical value for T_{error} of 0.62°C. The new calibration curve is shown in Figure 18.

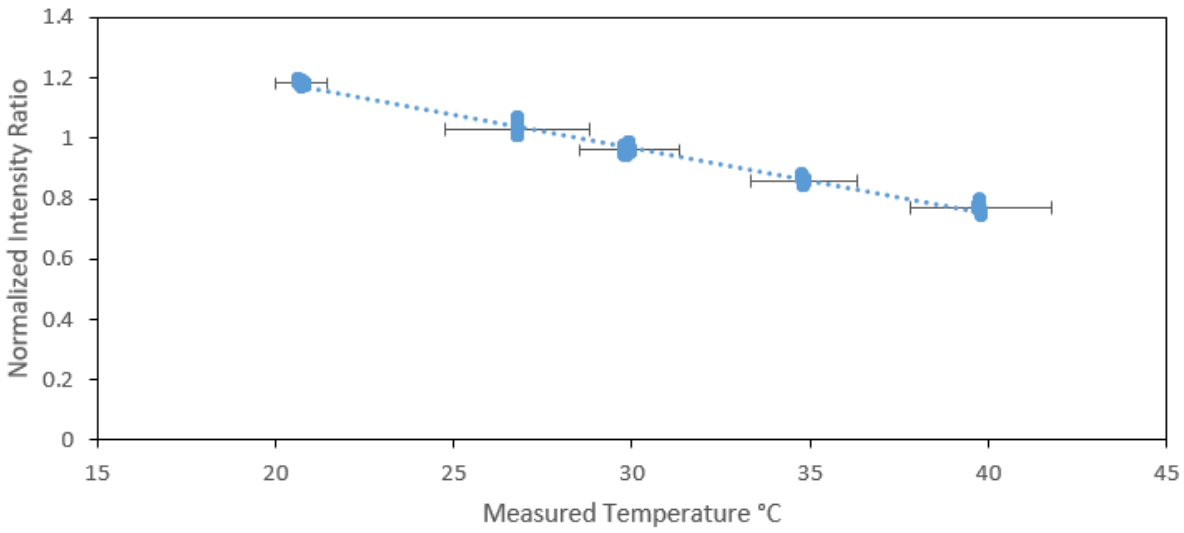

Figure 18 Normalized calibration curve.

The normalized calibration curve has an R squared value of 0.985. Eq. 10 was again used to find error bars for the calibration curve, except average calculated temperatures from the normalized temperature images were used. The confidence intervals for the two calibration curves were identical for the corresponding measurement temperatures. The equation for temperature, Eq. 11, is modified to use the normalized intensity ratio. The new temperature equation is given in Eq. 15.

$$T = \frac{\Omega - a}{b} \tag{15}$$

Using the new temperature equation, the same image used in the temperature image shown in Figure 17 was replotted and shown in Figure 19.

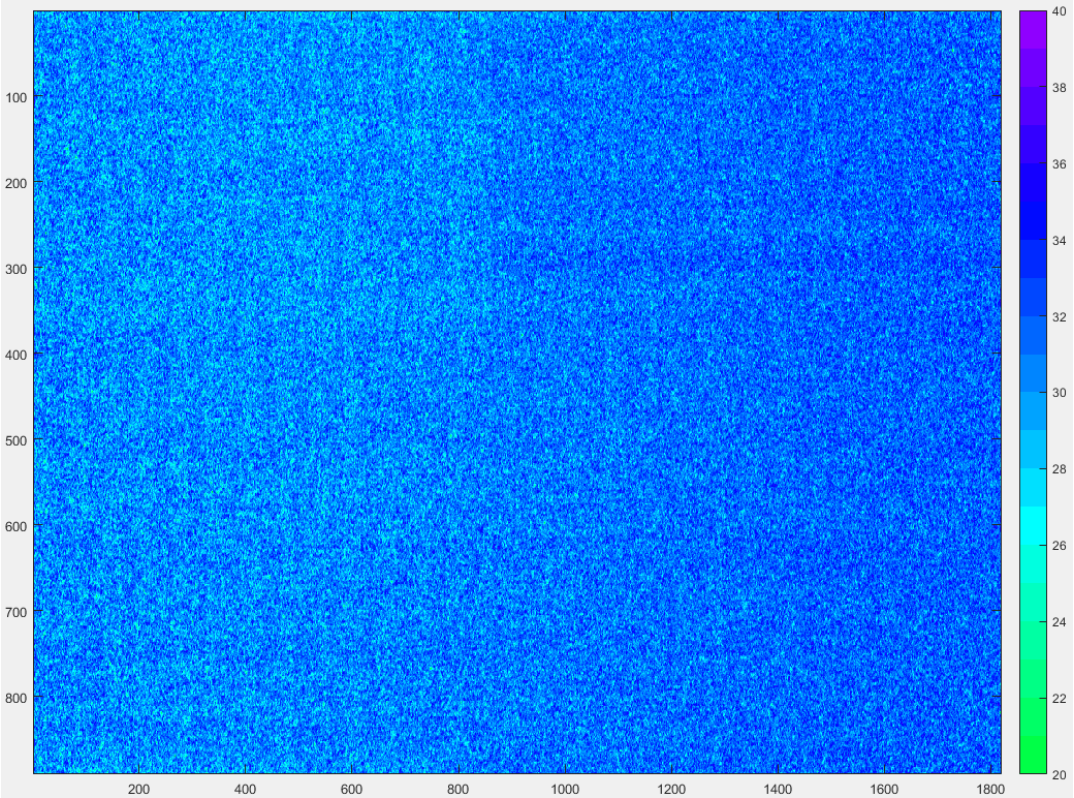

Figure 19 Temperature image at 30°C based on normalized calibration curve.

The figure shows the benefit of normalizing the intensity ratios. The optical spots that appear in Figure 17 have been removed. As a result, there is less error within the temperature image. To quantify the benefit of the normalization process and determine the accuracy of the temperature measurement system, the error within images before and after normalization was determined. Temperature plots were made for each image set with and without using normalization. Error within an image was determined using the standard deviation of the calculated image temperature values. The standard deviation within an image was calculated for the entire set of temperature images for each combination of temperature and path length with

normalized and non-normalized images. The normalized and non-normalized standard deviations were then averaged. In addition, the average temperature was determined for each image and the corresponding measured temperature was subtracted from the averages. The average of the absolute values of these errors was then determined. To determine how using reduced spatial resolution would improve the accuracy of the system, blocks of pixel values of the temperature images were averaged to determine the error for reduced resolution images. The results of the error calculations for non-normalized images are shown in Table 4 and for normalized images are shown in Table 5. The pixel resolution column refers to the number of measurement points in a temperature image, where the top row is the number of pixels in the original temperature image. The spatial resolution refers to the dimensions of the pixel for each resolution.

Table 4 Temperature error and pixel to pixel variance in non-normalized temperature images.

Pixel Resolution	Spatial Resolution (μm)	Standard Deviation (°C)	Error Between Temp Avg and Measured Temp (°C)
1820x890	10x10	±1.906	0.612
910x445	21x20	±1.633	0.840
364x178	52x51	±1.216	0.634
182x89	104x102	±1.068	0.598

Table 5 Temperature error and pixel to pixel variance in normalized temperature images.

Pixel Resolution	Spatial Resolution (μm)	Standard Deviation (°C)	Error Between Temp Avg and Measured Temp (°C)
1820x890	10x10	±1.678	0.692
910x445	21x20	±1.370	0.654
364x178	52x51	±0.876	0.650
182x89	104x102	±0.625	0.648

Overall the results from both error calculations show that the amount of variance decreases as the spatial resolution is decreased. However, decreasing the resolution also increases the

amount of error between measured temperature and calculated temperature. Comparing the results shown in Table 3 and Table 4 shows that the normalized images have less pixel to pixel variance than when normalization is not applied. The error between measured and calculated temperature also decreased slightly with image normalization at higher resolutions. The total system error can be found by adding the absolute values of the standard deviation and the measured temperature error. At full resolution, the total error is ±2.4°C. Using a lesser resolution of 104x102µm, the system error is found to be 1.3°C, or half the full resolution error.

Figure 20 shows a normalized temperature image from the other four calibration temperatures. The temperature images show some system noise with values varied around the mean temperature.

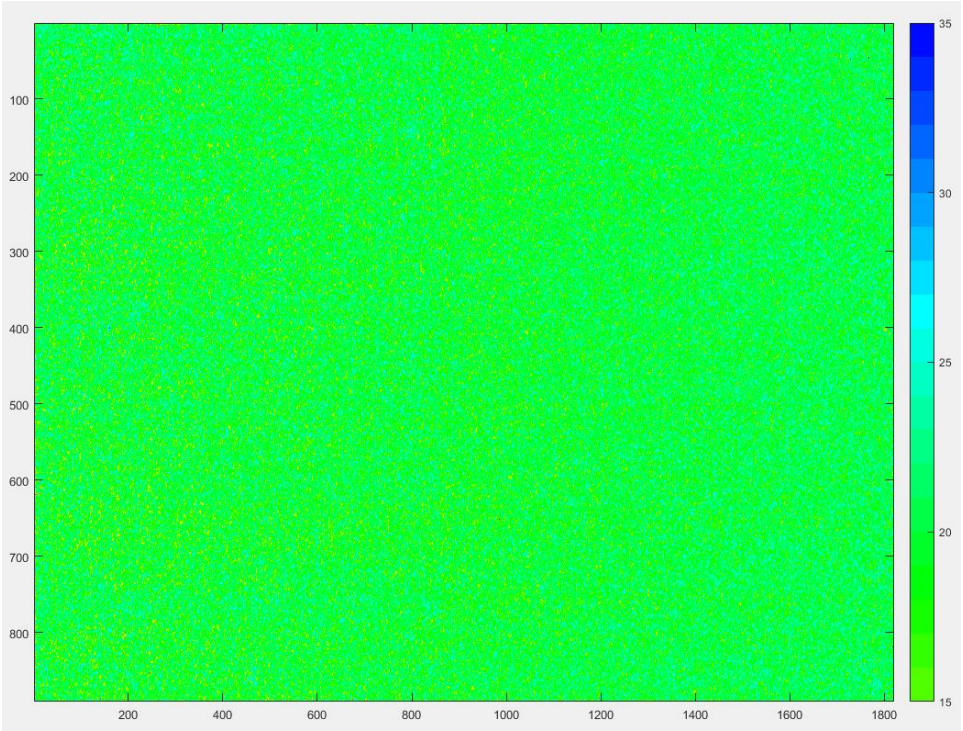

(a)

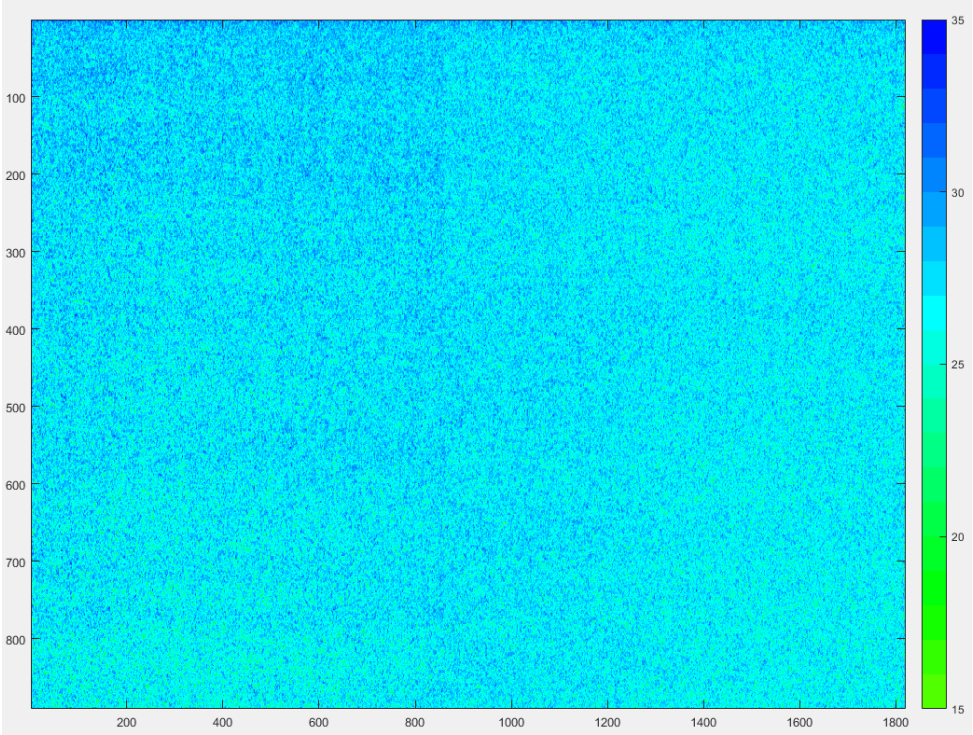
100
200
300
400
500
600
700
800
200
400
600
800
1000
1200
1400
1600
1800
35
30
25
20
15

(b)

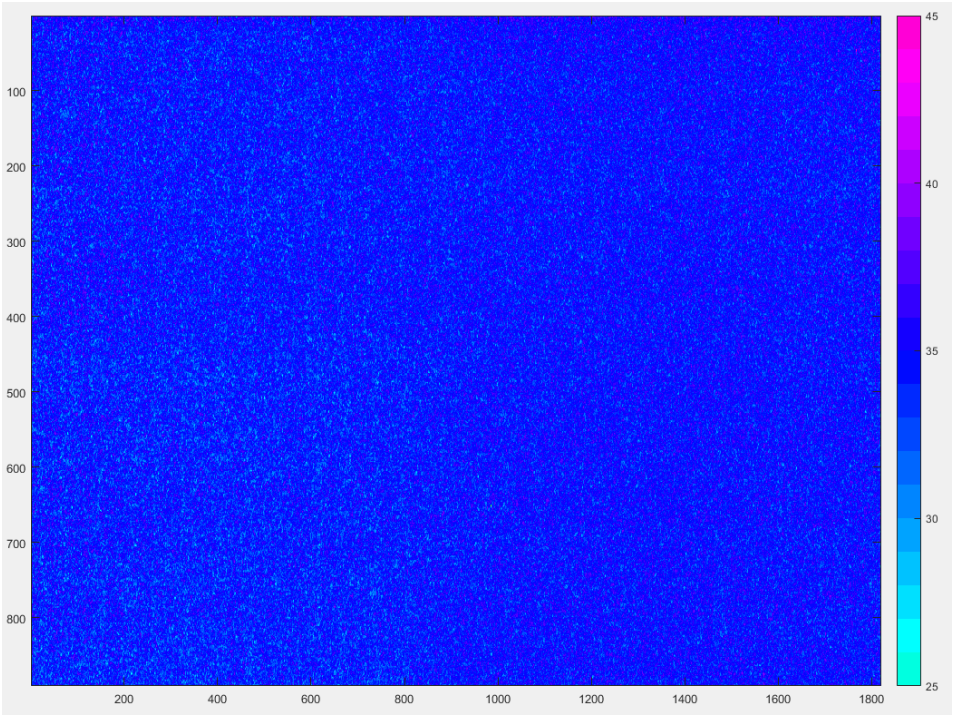
100
200
300
400
500
600
700
800
200
400
600
800
1000
1200
1400
1600
1800
45
40
35
30
25

(c)

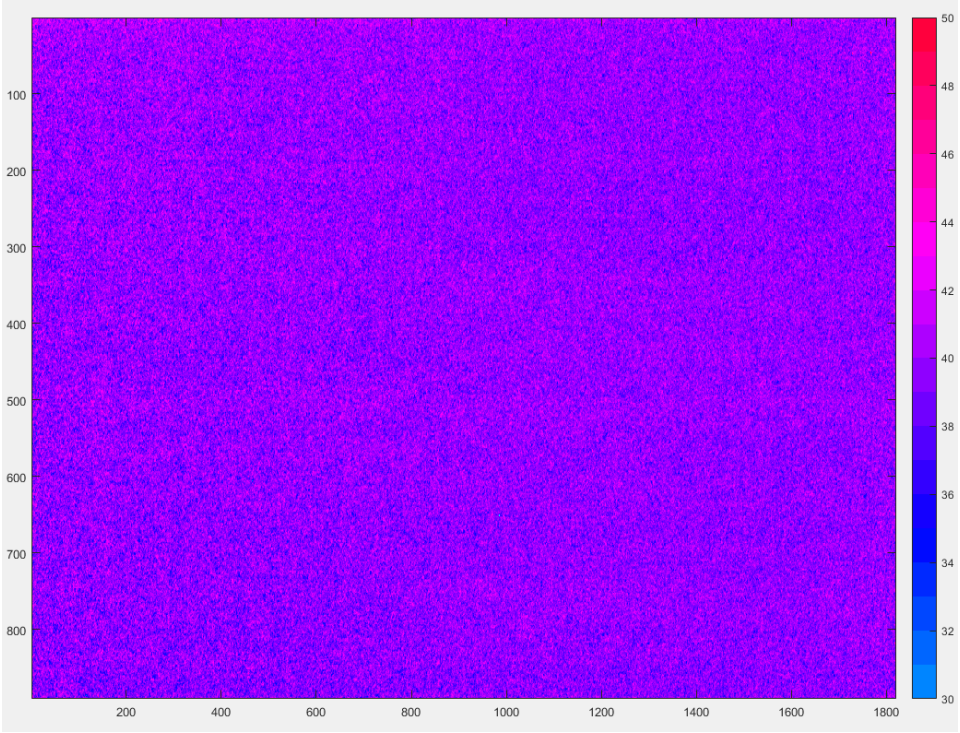

(d)

Figure 20 Temperature images from calibration. The images are representative images of the: (a) 20°C, (b) 26.9°C, (c) 35°C, and (d) 40°C calibration images.

The full code for calculating temperature images is shown in the Determine Image Temperatures section of Appendix A.

The next step was to take temperature measurements using the newly calibrated measurement system. The system was used to measure a temperature gradient within the glass tank used in the calibration setup. The gradient was created by heating the solution in the tank and then placing the bottom of the tank in ice water. This setup limited natural convection and so created a stronger temperature gradient. A schematic of the temperature gradient setup is shown in Figure 21.

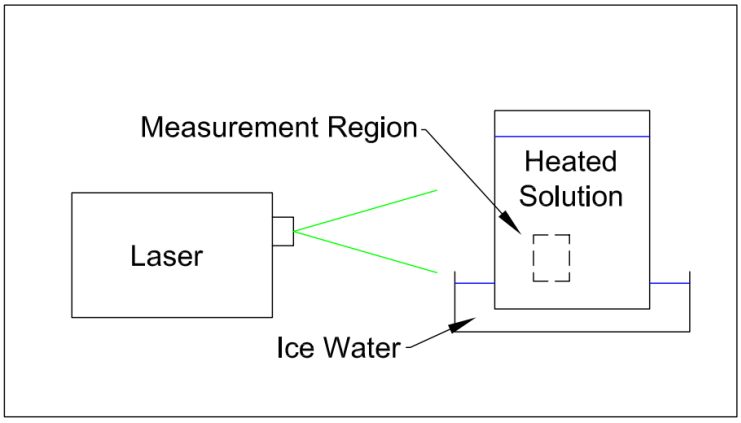

Figure 21 Schematic of temperature gradient setup.

The bottom of the viewing window was approximately 3cm from the bottom of the tank. The ice water line extended up the tank wall between 2 and 2.5cm. According to measurements taken by two thermocouples, the temperature gradient at the height in the tank that the measurement was taken was as high as 9°C. The measurement taken using the measurement system was off by a couple degrees. This is believed to be due to the fact that the thermocouples weren't placed in the measurement window. As a result, the fluid that the thermocouples were measuring was not the same temperature as the fluid the measurement system was viewing. A temperature image from this measurement is shown in Figure 22 with the temperature scale in degrees Celcius to the right of the image. The image is oriented so that the top of the image is closest to the top of the tank.

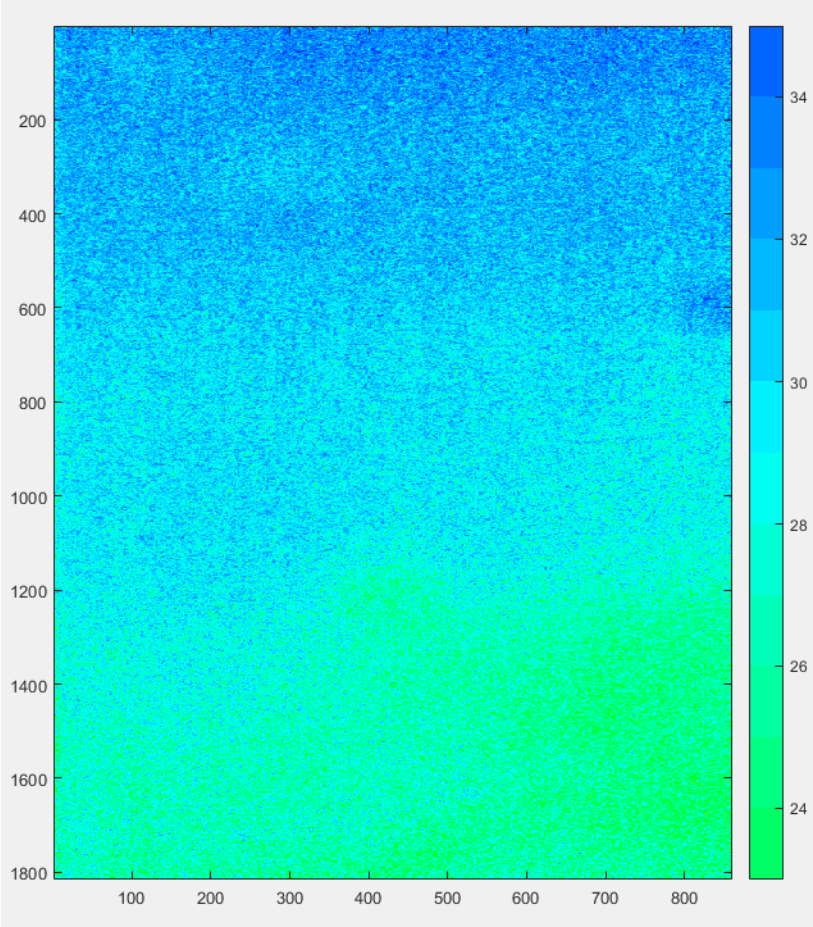

Figure 22 Image of temperature gradient.

The image shows that the ice bath setup was able to induce a temperature gradient visible in a 2cm height window. It was decided to take a second set of temperature measurements to show the change in the temperature gradient over time. The same ice bath setup was used for this second set of measurements. The bath was again heated to 40°C. Figure 23 shows both normalized (left) and non-normalized temperature images (right), taken at intervals after the tank was placed in the ice bath.

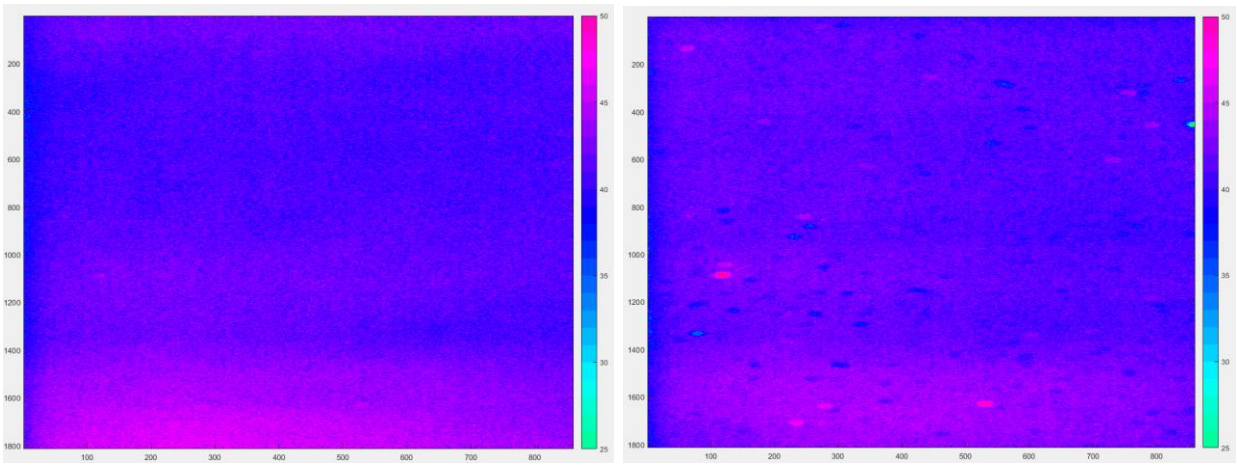

(a)

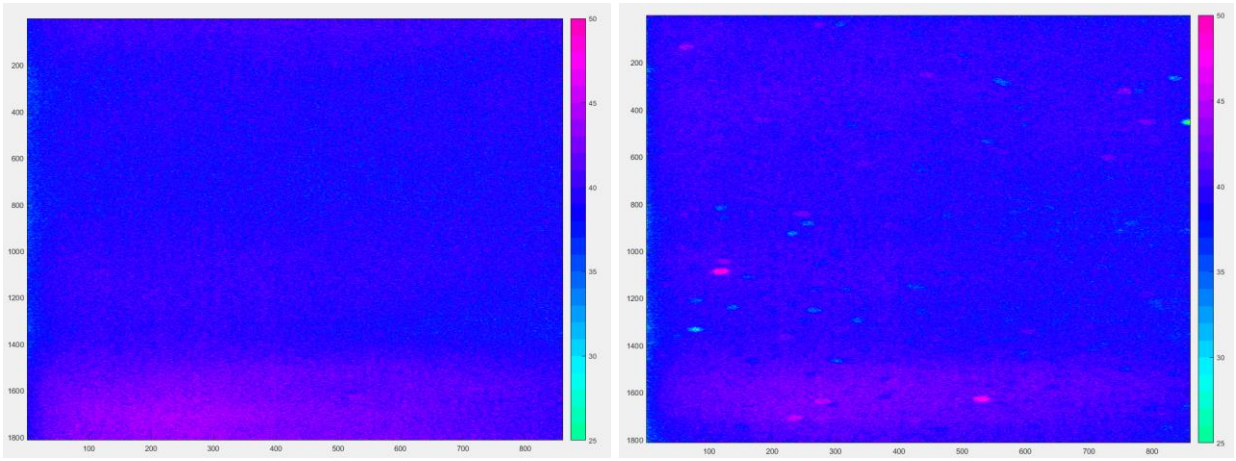

(b)

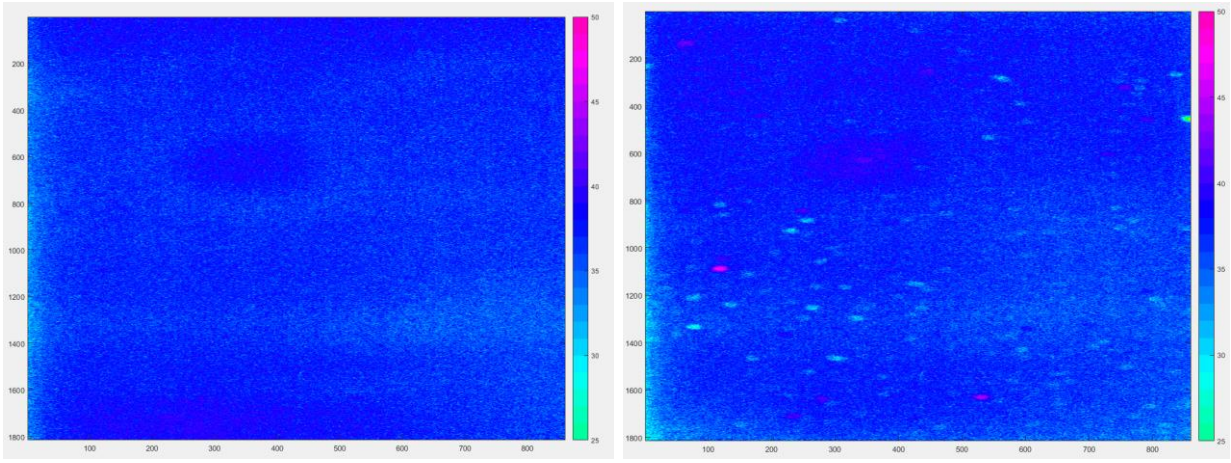

(c)

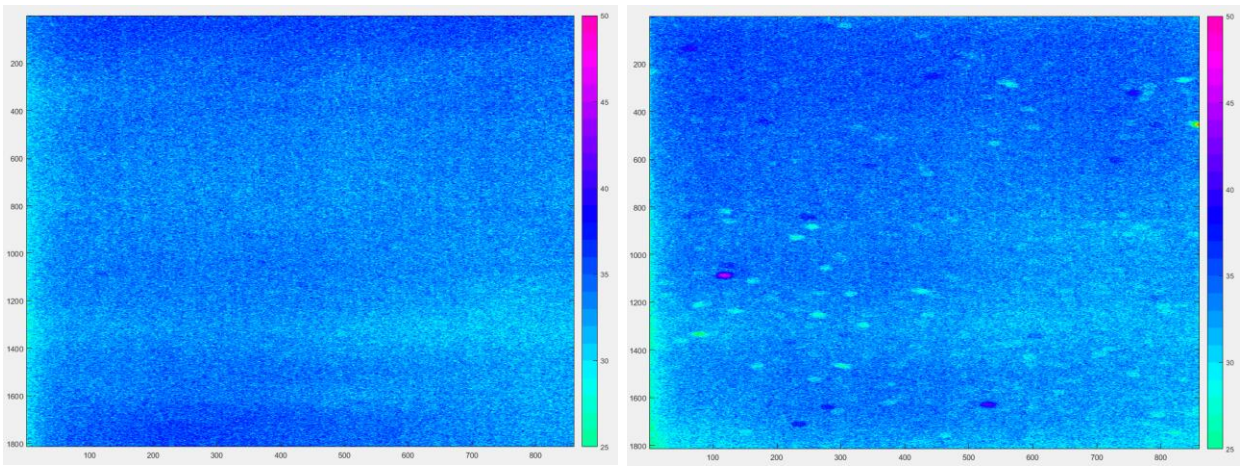

(d)

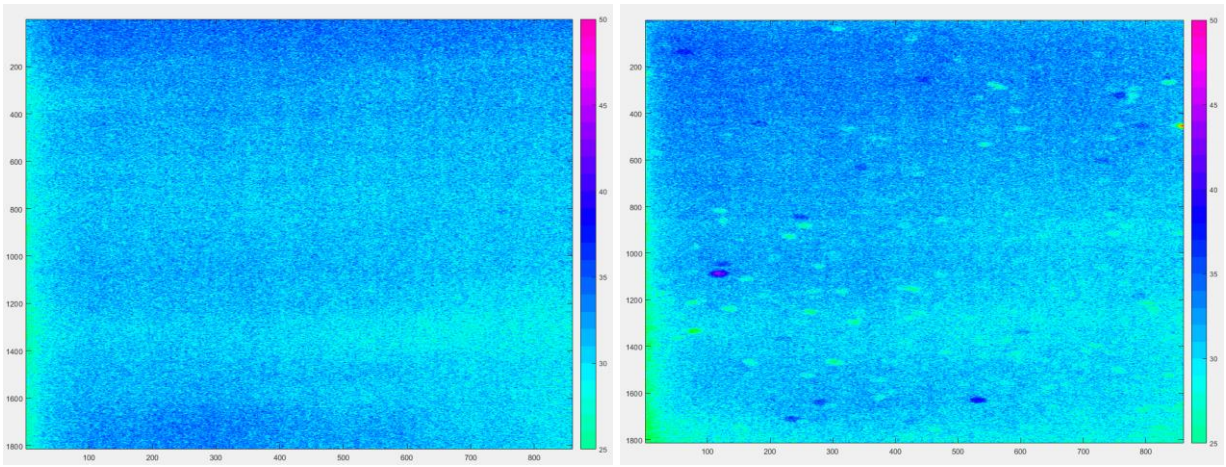

(e)

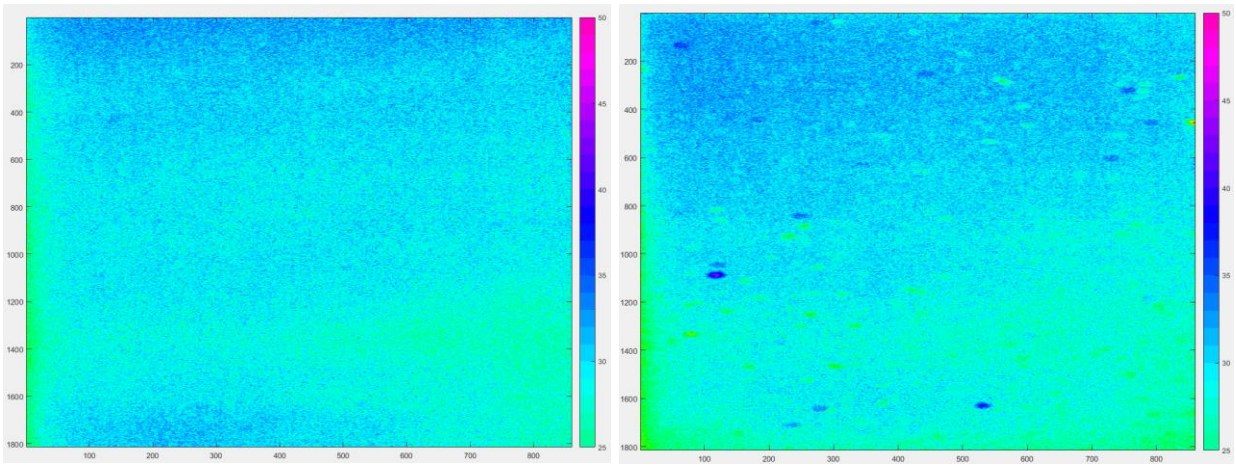

(f)

Figure 23 Temperature images taken after the water tank was added to the ice bath. Normalized images are shown on the left and non-normalized on the right. Temperature images are shown at times of: (a) t=0, (b) t=10min, (c) t=25min, (d) t=35min, (e) t=45min, and (f) t=55min.

The temperature images show the expected result that the overall temperature decreases in each consecutive image. The images also show patterns that appear in all the images. The most prominent of these is a horizontal line of lower temperature than the surrounding temperatures that stretches across the entire image between the 1200 and 1400 pixel height markings with the right side of the line spreading out to be much thicker. The patterns appear in both the normalized and non-normalized images and seem consistent between the two sets. The shape of the pattern stays constant over time, but their temperature decreases as the temperature of the entire image and the tank decreases. Because the shape of these features doesn't change over the course of the measurement, they must be the result of an optical feature. It was assumed that all optical features would be removed with image normalization. However, this temperature measurement result seems to show that image normalization removes small optical features, but not the larger patterns within the image and the measurement system.

The average temperature in the temperature images at 13 different times during the measurement were calculated and plotted against time. Temperature measurements taken every five minutes from just after the tank was placed in the bath to 55 minutes after the tank was placed in the water are plotted. The average thermocouple reading from two thermocouples that were at the same height as the measurement window and were taken at the same time as the temperature images were also plotted. The resulting graph is shown in Figure 24. Three thermocouple measurements are not shown because they were missed during the measurement process.

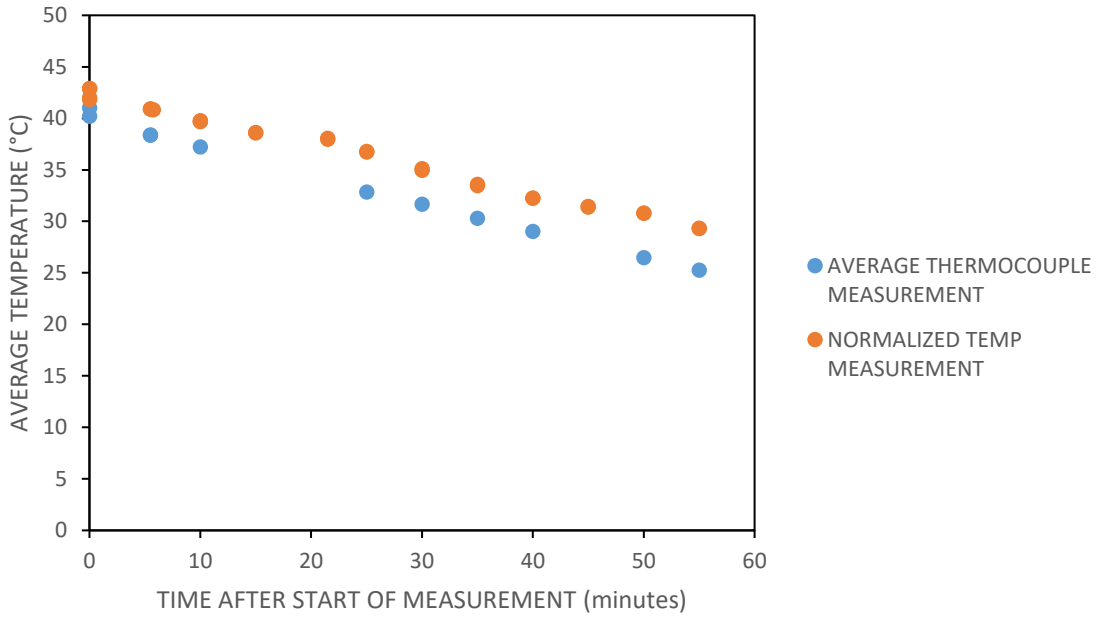

Figure 24 Plot of the average temperature of the temperature images and thermocouple readings over the life of the measurement.

The averages for normalized and non-normalized images were both calculated and found to give very close to the same result at each time step, so only the normalized temperature averages are shown. There is an offset though, between the thermocouple measurements and the PLIF measurements. There are likely two reasons for this. The average global temperature error is 0.6°C, which could account for some of the error. In addition, the system was mainly being cooled from the walls of the tank. There was not much fluid beneath the tank. Therefore, if the thermocouples were closer to the wall than the viewing window, then the point measurements would be cooler than the temperature measurements taken by the measurement system. The slopes for both data sets are very similar though, which means that the two different spots in the measurement volume at the same height were cooling at similar rates.

The temperature measurements and error calculations completed in this section show that the measurement system works well on a global level to measure temperature and temperature

trends. However, more work needs to be completed to try and reduce the local temperature error. The first step will be to determine what is causing the global temperature patterns and try and correct for these features.

Chapter 6 - Summarized Calibration Procedure

All measurement systems require precise calibration to give accurate readings. This measurement system is no different. This thesis described the development of a calibration procedure and measurement system, but every time the dye solution is changed, the system must be recalibrated. This is true if it is determined the concentration of either dye should be changed or if the solvent, distilled water and methanol, is changed. A new calibration would also need to be completed if some of the fluid in the tank evaporated because the concentration of the dyes would be changed. This section will give a detailed description of the calibration procedure for the developed two-color ratiometric PLIF thermometry system.

The first step is to make a stock solution of the chosen dyes. RhB and RH110 dyes were chosen in this thesis, but any combination of fluorescent dyes that meet the criteria specified in the section Experimental Setup will work. It was determined that 25mg/L was close to the upper solubility limit for both RHB and R110. To make a stock solution of this concentration, 25mg of each fluorescent dye powder were measured out using an analytical balance. The measured dye was added to a solute of 950mL distilled water and 50mL methanol. The solution was stirred until no solid dye was visible in the solution. After mixing the new stock, the concentration of each dye to be used in the proceeding calibration and measurements should be determined. A concentration of 0.125mg/L of RHB and 1mg/L RH110 was found to give the most consistent results during this work. Using these concentrations, one liter of solution can be created as follows. Measure out 980mL of distilled water. Add 20mL of the RHB stock solution using a graduated pipet. Mix this solution well. Then measure out 250mL of this solution and pour out the rest into a hazardous waste bin. The MSDS for both dyes states not to empty the chemical into drains because of harmful ecological effects. To the 250mL of solution, add 40mL of the RH110 stock solution and

710mL of distilled water. Mix this solution well. The dye solution is then ready to be used for calibration and measurements. Place the solution in a sealed container while storing and preparing the rest of the calibration setup. A solution of just RH110 should be mixed as well at the same concentration. This solution will be used to determine the signal crossing ratio M for RH110.

Next the measurement system should be placed, and its position fixed. The focal plane of the cameras can then be found by taking images of a target and moving the target until the images are in focus. One of these in focus images from each camera should be saved to use for image alignment. All images taken with the measurement system were viewed and saved using Bobcat GEV Player, the manufacturer recommended software. Two instances of the software are required, one to control each camera. The laser should be lined up so that the laser sheet will be coplanar with the focal plane. Next the measurement volume for the current temperature measurements should be chosen and placed at the intersection of the measurement system line of site and the laser path. Measuring from the inside of the front wall (closest to the measurement system) to the laser path, choose three locations for the tank so that measurements can be taken at three different path lengths. Note the location of the front of the tank at these three path length locations. Path lengths of 1, 2, and 3 inches were chosen for the current work and the front edge of the hot plate that the water tank was resting on was used to mark the path length locations. Once all the pieces of the measurement system are placed, the RH110 dye solution can be added to the measurement volume.

Next, the settings for the two cameras should be chosen in GEV Player. The settings for the current work were that the cameras used external trigger mode for image capture. One of the cameras was set to have a trigger strobe with a delay of 2000μs. This strobe acts as the trigger for

one of the laser lamps. The cameras were each set to single trigger mode and an exposure time of 3500μs. These settings need to be saved for future sessions.

Once the camera settings are saved, the function generator needs to be setup as described in the section Experimental Setup. 50 ohm coaxial cable was used to connect the function generator to the cameras and connect one of the cameras to the laser to deliver trigger signals. Thermocouples need to be calibrated to determine the temperature of the solution. The average temperature read by three thermocouples was used for the current work. Once the thermocouples are calibrated, place them in the measurement volume so that the end of the temperature sensor is 0at the same height as the viewing window of the measurement system. For calibration, make sure that all the lights in the room are off or covered and that the computer is facing away from the setup.

Calibration starts by determining the crossover ratio M. Move the measurement volume to the first path length. Turn on the laser. Once the laser has warmed up, the first set of measurements can be taken. Take a set of 30 images with each camera. Take image sets at four other path lengths. Then, remove the RH110 solution from the measurement volume, put it back in its container, and clean the measurement volume thoroughly. Calibration of the two-dye solution can then commence.

Room temperature can be one of the five temperatures used for calibration measurements. Take a set of 30 images with each camera. At the same time, record the temperature reading from the thermocouples. Do the same for the other two path lengths. Next, use a hot plate or temperature bath to heat the solution to the next temperature. If using a hotplate, the solution should be heated slowly and stirred using a magnetic stirrer to keep the temperature as even in the measurement volume as possible. Once the thermocouples are reading a constant temperature, the

second set of temperature measurements can be taken. Again, take 30 sets of images at the three different path lengths. Repeat this procedure for the other three calibration temperatures. A set of background images should also be obtained for background subtraction by the MATLAB code.

Next, the Image Alignment code should be used to find a translation to use for all camera images. Then all 15 image sets from temperature calibration and all five image sets from the cross over ratio calibration should be run through the Calculate Average Image Intensities code. The average intensity values from the RH110 solution image sets should be formed into the ratio M defined in Eq. 3 and plotted vs path length. A linear least squares model can be used to form an equation for M with respect to path length.

Next, the two-dye solution should be calibrated. The average intensity values from the Calculate Average Image Intensities code, along with the path length and average temperature for each two-dye solution image set should be recorded in a spreadsheet in four separate columns. A cell should be designated for the extinction coefficient ψ, a, and b. Then Eq. 5 should be placed in a column and calculated for each image set, with I_{110} being the output. Another column should be used to calculate I_B using the top of the fraction in Eq. 4. The value of M in Eq. 4 should be input as the equation calculated using the RH110 solution calibration values with respect to path length. The intensity ratio R can then be calculated by dividing I_B by I_{110} for each image set. Next, $T_{calculated}$ should be determined for each image set using Eq. 8. T_{error} should be found in the last column using Eq. 9. In a cell above the T_{error} column, the average of the column should be found. A solver can then be used to minimize T_{error} by changing ψ, a, and b. Once these variables are determined, the system calibration is complete. These variables can then be input into the Determine Image Temperatures code to find local temperatures and temperature images.

A separate curve needs to be created if image normalization is to be used. To do this, a set of normalization images needs to be taken. These images should be a set of constant temperature images taken in the measurement volume. The exact temperature doesn't matter if it is constant across the measurement window. The path length of these images should be recorded.

The steps to create the spreadsheet for determining ψ, a, and b are the same as for the non-normalized curve until the columns of the corrected intensity values I_B and I_{110} are created. Once that is completed, then the average image intensity values for the normalization images should be determined using the Calculate Average Image Intensities code. The average of the average intensities for each camera can then be calculated. These two values along with the path length of the normalization images should be placed in the spreadsheet. Again using Eq. 4 for camera 1 values and Eq. 5 for camera 2 values, the corrected intensities should be calculated for the two average normalization intensities. The ratio, Φ, is found by dividing the corrected, normalized I_{110} by the corrected, normalized I_B. Now, the normalized intensity ratio can be found using Eq. 13 and plugging in the corrected intensity values for each image set and Φ. $T_{calculated}$ can be determined using Eq. 14. Then T_{error} for each image set can be found using Eq. 15. In a cell above the T_{error} column, the average of the column is found again. The solver is again used to minimize the average T_{error} by changing the variables ψ, a, and b. Determine Image Temperatures code is used to find normalized local temperatures and temperature images as well, but the variables ψ, a, and b should be input into the correct set of code variables and the variable "normalization" should be set to 1. A new normalization set of images and, as a result, a new normalized calibration curve and set of variables should be found every time something with the measurement optics changes. This includes taking the measurement system apart, cleaning the components, or replacing a component.

Chapter 7 - Conclusion

Planar laser induced fluorescence is a versatile technique for measuring many different fluid properties. This work described the process of calibrating a PLIF temperature measurement system that relates the fluorescent intensity ratio of RHB and RH110 dyes to temperature. By examining the equation for fluorescence, the benefit of using a ratio of the intensity signals from a temperature sensitive and temperature insensitive dye was shown. The ratio is able to account for variances in laser intensity within the measurement plane and between consecutive laser pulses. The fluorescent dyes for this experimental setup were chosen based on criteria set by available equipment and the experimental technique. The absorption and emission spectra of the selected dyes were examined to determine appropriate optical filters for the cameras. The shape of the absorption and emission spectra of the chosen dyes necessitated modifications to the fluorescence intensity ratio equation to account for signal crossing of the dyes and reabsorption of the I_{110} signal. Corrections to the ratio equation were developed and the parameters needed to perform those corrections were determined. Calibration image sets were taken at five different temperature and three different path lengths. The ratio of $I_{110\text{-}LP}$ to I_2 signals, M, was determined using a similar calibration procedure.

Image processing steps were determined to damp out the banding pattern in images from camera 2. Background subtraction and image alignment were also performed. The viewing window for the aligned images was 1.9x0.91cm. Processed images were then used to determine average image intensities for all the calibration images. These average intensities were used to determine an extinction coefficient, ψ, and a calibration curve. Initial temperature images were produced with this calibration curve. These initial images were found to have spots of high and low temperature. A normalization process and normalized calibration curve were developed to

account for these spots. The normalized images were shown to remove the spots and have less variance in their temperature values. The overall temperature error between measured and average calculated temperature was found to be 0.6°C. The system is capable of taking instantaneous temperature measurements at a resolution of 10x10μm with an error of ±2.4°C (inter-image deviation plus measured vs calculated temperature error). The system error can be reduced to ±1.3°C by reducing the image resolution to 104x102μm. Once the system was calibrated, it was used to measure a temperature gradient induced by placing a heated water tank in an ice bath. The temperature measurement showed an optical pattern that was not corrected by image normalization. The next steps for this research will be to try and refine the local temperature measurements and remove the optical pattern. Finally, a finalized, step-by-step calibration procedure for the developed two-color ratiometric thermometry technique was described.

References

Abram, C., Pougin, M., Fond, B., & Beyrau, F. (July, 2016). Temperature imaging in liquids using ZnO thermographic phosphor particles. Paper presented at the *Laser Applications to Chemical, Security and Environmental Analysis, LACSEA 2016, July 25, 2016 - July 28,* OSA.

Amiri, S., Taher, R., & Mongeau, L. G. (2014). Experimental study of the oscillatory velocity and temperature near a heated circular cylinder in an acoustic standing wave. *International Journal of Heat and Mass Transfer, 69*, 464-472.

Andreini, A., Cocchi, L., Facchini, B., Mazzei, L., & Picchi, A. (2018). Experimental and numerical investigation on the role of holes arrangement on the heat transfer in impingement/effusion cooling schemes. *International Journal of Heat and Mass Transfer, 127*, 645-659.

New Mexico State University. (2006). *Beer-lambert law*. Retrieved from https://web.nmsu.edu/~kburke/Instrumentation/BeersLaw.html

California Institute of Technology. (2018). *Brief history of thermoelectrics*. Retrieved from http://www.thermoelectrics.caltech.edu/thermoelectrics/history.html

Bruchhausen, M., Guillard, F., & Lemoine, F. (2005). Instantaneous measurement of two-dimensional temperature distributions by means of two-color planar laser induced fluorescence (PLIF). *Experiments in Fluids, 38*(1), 123-131.

Chamarthy, P., Garimella, S. V., & Wereley, S. T. (2010). Measurement of the temperature non-uniformity in a microchannel heat sink using microscale laser-induced fluorescence. *International Journal of Heat and Mass Transfer, 53*(15-16), 3275-3283.

Davidson, M., Herman, B., Frohlich, V., Lakowicz, J., Murphy, D. & Spring, K. (2015). *Fluorescence microscopy: Basic concepts in fluorescence*. Retrieved from https://micro.magnet.fsu.edu/primer/techniques/fluorescence/fluorescenceintro.html

Estrada-Pérez, C. E., Hassan, Y. A., & Tan, S. (2011). Experimental characterization of temperature sensitive dyes for laser induced fluorescence thermometry. *Review of Scientific Instruments, 82*(7)

Euler, M., Zhou, R., Hochgreb, S., & Dreizler, A. (2014). Temperature measurements of the bluff body surface of a swirl burner using phosphor thermometry. *Combustion and Flame, 161*(11), 2842-2848.

Scientific Volume Imaging. (2018). *Fluorescence*. Retrieved from https://svi.nl/Fluorescence

National Instruments. (2016, Mar 30). *Taking Temperature Measurements with RTDs: How-To Guide*. Retrieved from http://www.ni.com/tutorial/7115/en/

Kim, H. J., & Kihm, K. D. (2001). (2001). Application of a two-color laser induced fluorescence (LIF) technique for temperature mapping. Paper presented at the *2001 ASME International Mechanical Engineering Congress and Exposition, November 11, 2001 - November 16, 369*(7) 335-341.

Kowalewski, T. A. (2001). Particle image velocimetry and thermometry using liquid crystal tracers. *DLR-Mitteilung*, (3), 181-190.

Lacassagne, T., Simoëns, S., El Hajem, M., & Champagne, J. -. (2018). Ratiometric, single-dye, pH-sensitive inhibited laser-induced fluorescence for the characterization of mixing and mass transfer. *Experiments in Fluids, 59*(1)

Li, P., Eckels, S. J., Mann, G. W., & Zhang, N. (2018). A method of measuring turbulent flow structures with particle image velocimetry and incorporating into boundary conditions of large eddy simulations. *Journal of Fluids Engineering, Transactions of the ASME, 140*(7)

Mootz, J., & Mathews, L. *Displaying and stretching 16-bit per band digital imagery*. Retrieved from https://www.fsa.usda.gov/Assets/USDA-FSA-Public/usdafiles/APFO/support-documents/pdfs/film_vs_digital_linear_non-linear_stretches.pdf

Schreivogel, P., Abram, C., Fond, B., Straußwald, M., Beyrau, F., & Pfitzner, M. (2016). Simultaneous kHz-rate temperature and velocity field measurements in the flow emanating from angled and trenched film cooling holes. *International Journal of Heat and Mass Transfer, 103*, 390-400.

Thermo Fisher Scientific. *Fluorescence fundamentals*. Retrieved from https://www.thermofisher.com/us/en/home/references/molecular-probes-the-handbook/introduction-to-fluorescence-techniques.html

Vogt, J., & Stephan, P. (2012). Using microencapsulated fluorescent dyes for simultaneous measurement of temperature and velocity fields. *Measurement Science and Technology, 23*(10)

West, T. (2012). *Development and testing of temperature-sensitive beads for simultaneous thermometry and velocimetry*

Xu, C. Y., Cai, X. S., Liu, G. L., & Yan, F. N. (2010). (2010). Measurement of water temperature using planer laser induced fluorescence. Paper presented at the *AIP Conference Proceedings, , 1207* 189-192.

Yamaguchi, E., Natrajan, V. K., & Christensen, K. T. (2006). (2006). Development of a two-dye LIF technique for measuring fluid temperature fields in microfluidic devices. Paper presented at the - *European Fluids Engineering Division Summer Meeting, FEDSM2006, July 17, 2006 - July 20, 2006, 2 FORUMS* 535-540.

Yi, S. J., Kim, H. D., & Kim, K. C. (2014). Decay-slope method for 2-dimensional temperature field measurement using thermographic phosphors. *Experimental Thermal and Fluid Science, 59,* 1-8.

Zhang, J. M., Dong, S. J., & Wu, Y. (2015). (2015). Measurement of temperature and flow field in cabin on natural convection. Paper presented at the *International Conference on Frontier of Energy and Environment Engineering, ICFEEE 2014, December 6, 2014 - December 7,* 79-82.

Appendix A - MATLAB Code

Image Alignment

```
%IMAGE ALIGNMENT

clc;
close all;
%%
% Take a picture of a target with both cameras

% Importing alignment photos
Moving=imread('FILEPATH\CAMERA 1.tif');
Fixed=imread('FILEPATH\CAMERA 2.tif');

% Display both alignment images
figure, imshow(Fixed);
figure, imshow(Moving);


% Define Translation for Camera 1 image
xtranslation=220;
ytranslation=-105;

Moved=imtranslate(Moving,[xtranslation,ytranslation]);

% Show translated camera 1 image on top of camera 2 image
figure;
imshowpair(Moved,Fixed);
title('default registration');

% Check manual alignment with registered alignment
[optimizer,metric]=imregconfig('Multimodal');
registered=imregister(Moving,Fixed,'translation',optimizer,metric);
figure;
imshowpair(registered,Fixed);
title('default registration');

%If the manual and automatic intensity alignment give the same result, then
%you have found the proper image alignment
```

Calculate Average Image Intensities

```
clc;
close all;
clear;
%%
% Import images
low=1;
high=30;
N=high-low+1;
```

```
cd 'FILE PATH\FOLDER WITH CAMERA 2 IMAGES';%sets current folder
k = categorical(1,N);
L=1920;
W=1080;
C=zeros(W,L,1);
D=zeros(W,L,1);
for n=low:high
    if n<10
    k(n-low+1)=strcat('0000000',num2str(n),'.tif');
    S=char(k);
    C = cat(3,C,imread(S(n-low+1,:)));
    end
    if n>=10
    k(n-low+1)=strcat('000000',num2str(n),'.tif');
    S=char(k);
    C = cat(3,C,imread(S(n-low+1,:)));
    end
end

cd 'FILE PATH\FOLDER WITH CAMERA 1 IMAGES';%sets current folder
k1 = categorical(1,N);
for m=low:high
    if m<10
    k1(m-low+1)=strcat('0000000',num2str(m),'.tif');
    S1=char(k1);
    D = cat(3,D,imread(S1(m-low+1,:)));
    end
    if m>=10
    k1(m-low+1)=strcat('000000',num2str(m),'.tif');
    S1=char(k1);
    D = cat(3,D,imread(S1(m-low+1,:)));
    end
end

%Import background images
cd 'FILE PATH\FOLDER WITH CAMERA 2 BACKGROUND IMAGES';%sets current folder
low=1;
high=30;
k = categorical(1,N);
r=zeros(W,L,1);
q=zeros(W,L,1);
for n=low:high

    if n<10
    k(n-low+1)=strcat('0000000',num2str(n),'.tif');
    S=char(k);
    r = cat(3,r,imread(S(n-low+1,:)));
    end
    if n>=10
    k(n-low+1)=strcat('000000',num2str(n),'.tif');
    S=char(k);
    r = cat(3,r,imread(S(n-low+1,:)));
    end
end

cd 'FILE PATH\FOLDER WITH CAMERA 1 IMAGES';%sets current folder
```

```
k1 = categorical(1,N);
for m=low:high
    if m<10
    k1(m-low+1)=strcat('0000000',num2str(m),'.tif');
    S1=char(k1);
    q = cat(3,q,imread(S1(m-low+1,:)));
    end
    if m>=10
    k1(m-low+1)=strcat('000000',num2str(m),'.tif');
    S1=char(k1);
    q = cat(3,q,imread(S1(m-low+1,:)));
    end
end

%% remove blank front array
C(:,:,1)=[];
D(:,:,1)=[];
r(:,:,1)=[];
q(:,:,1)=[];

%% Background Subtraction
C=C-r;
D=D-q;

%% Image Translation (From image alignment)
up=xtranslation;
over=ytranslation;

E(:,:,:)=imtranslate(D(:,:,:),[over,up]);
F(:,:,:)=E(1:(1080+up),(1+over):1920,:);
G(:,:,:)=C(1:(1080+up),(1+over):1920,:);
%% BLOCK AVERAGE
for a=1:N
    for b=2:(1920-over-1)
     for z=2:(1080-up-1)
         G(z,b,a)=mean(mean(G(z-1:z+1,b-1:b+1,a)));
     end
    end
    for b=1:(1920-over)
        G(1,b,a)=mean(mean(G(1:2,b,a)));
        G(1080-up,b,a)=mean(mean(G(1080-up-1:1080-up,b,a)));
    end
    for z=1:(1080-up)
        G(z,1,a)=mean(mean(G(z,1:2,a)));
        G(z,1920-over,a)=mean(mean(G(z,1920-over-1:1920-over,a)));
    end
end

%% Exporting data

%Camera image local 1920 Average, Std, High, Low
average1920=zeros(N,1);
std1920=zeros(N,1);
high1920=zeros(N,1);
low1920=zeros(N,1);
```

```
for a=1:N
average1920(a,1)=mean(mean(G(:,:,a)));
std1920(a,1)=std2(G(:,:,a));
high1920(a,1)=max(max(G(:,:,a)));
low1920(a,1)=min(min(G(:,:,a)));
end
disp(average1920);
disp(std1920);

summary1920=zeros(N,3);
summary1920(:,1)=average1920(:,1);
summary1920(:,2)=std1920(:,1);
summary1920(:,3)=high1920(:,1);
summary1920(:,4)=low1920(:,1);
filename='C:\Users\Student\Desktop\1920SUMMARY';
xlswrite(filename,summary1920);

%Camera image local 1923 Average, Std, High, Low
average1923=zeros(N,1);
std1923=zeros(N,1);
high1923=zeros(N,1);
low1923=zeros(N,1);
for a=1:N
average1923(a,1)=mean(mean(F(:,:,a)));
std1923(a,1)=std2(F(:,:,a));
high1923(a,1)=max(max(F(:,:,a)));
low1923(a,1)=min(min(F(:,:,a)));
end
disp(average1923);
disp(std1923);

summary1923=zeros(N,3);
summary1923(:,1)=average1923(:,1);
summary1923(:,2)=std1923(:,1);
summary1923(:,3)=high1923(:,1);
summary1923(:,4)=low1923(:,1);
filename='C:\Users\Student\Desktop\1923SUMMARY';
xlswrite(filename,summary1923);
```

Determine Image Temperatures

```
clc;
close all;
clear;
%%
%If you want normalized images, set normilization=1, otherwise, 0
Normalization=1;
if normalization==1
    B=1.3904;
    A=0.019;
    psi=0.139;
else
    B=106.4205;
```

```
    A=0.1391;
    psi=0.1391;
end
PL=2;
onetenratio=0.1898*PL+1.7133;
low=5;
high=34;
N=high-low+1;
cd 'FILE PATH\FOLDER WITH CAMERA 2 IMAGES';%sets current folder
k = categorical(1,N);
L=1920;
W=1080;
C=zeros(W,L,1);
D=zeros(W,L,1);
for n=low:high
    if n<10
    k(n-low+1)=strcat('0000000',num2str(n),'.tif');
    S=char(k);
    C = cat(3,C,imread(S(n-low+1,:)));
    end
    if n>=10
    k(n-low+1)=strcat('000000',num2str(n),'.tif');
    S=char(k);
    C = cat(3,C,imread(S(n-low+1,:)));
    end
end

cd 'FILE PATH\FOLDER WITH CAMERA 1 IMAGES';%sets current folder
k1 = categorical(1,N);
for m=low:high
    if m<10
    k1(m-low+1)=strcat('0000000',num2str(m),'.tif');
    S1=char(k1);
    D = cat(3,D,imread(S1(m-low+1,:)));
    end
    if m>=10
    k1(m-low+1)=strcat('000000',num2str(m),'.tif');
    S1=char(k1);
    D = cat(3,D,imread(S1(m-low+1,:)));
    end
end

%Background subtraction
cd 'FILE PATH\FOLDER WITH CAMERA 2 Background IMAGES';%sets current folder
low=1;
high=30;
k = categorical(1,N);
r=zeros(W,L,1);
q=zeros(W,L,1);%may have an error later if camera converts back to 1928
pixels wide
for n=low:high

    if n<10
    k(n-low+1)=strcat('0000000',num2str(n),'.tif');
    S=char(k);
    r = cat(3,r,imread(S(n-low+1,:)));
```

```
    end
    if n>=10
    k(n-low+1)=strcat('000000',num2str(n),'.tif');
    S=char(k);
    r = cat(3,r,imread(S(n-low+1,:)));
    end
end

cd 'FILE PATH\FOLDER WITH CAMERA 1 Background IMAGES';%sets current folder
k1 = categorical(1,N);
for m=low:high
    if m<10
    k1(m-low+1)=strcat('0000000',num2str(m),'.tif');
    S1=char(k1);
    q = cat(3,q,imread(S1(m-low+1,:)));
    end
    if m>=10
    k1(m-low+1)=strcat('000000',num2str(m),'.tif');
    S1=char(k1);
    q = cat(3,q,imread(S1(m-low+1,:)));
    end
end

if normalization==1
PL1=1;
onetenratio1=0.1898*PL+1.7133;
cd 'FILE PATH\FOLDER WITH CAMERA 2 Normalization IMAGES';%sets current folder
k = categorical(1,N);
low=1;
high=30;
L=1920;
W=1080;
H=zeros(W,L,1);
I=zeros(W,L,1);
for n=low:high
    if n<10
    k(n-low+1)=strcat('0000000',num2str(n),'.tif');
    S=char(k);
    H = cat(3,H,imread(S(n-low+1,:)));
    end
    if n>=10
    k(n-low+1)=strcat('000000',num2str(n),'.tif');
    S=char(k);
    H = cat(3,H,imread(S(n-low+1,:)));
    end
end

cd 'FILE PATH\FOLDER WITH CAMERA 1 Normalization IMAGES';%sets current folder
k1 = categorical(1,N);
for m=low:high
    if m<10
    k1(m-low+1)=strcat('0000000',num2str(m),'.tif');
    S1=char(k1);
    I = cat(3,I,imread(S1(m-low+1,:)));
    end
    if m>=10
```

```
    k1(m-low+1)=strcat('000000',num2str(m),'.tif');
    S1=char(k1);
    I = cat(3,I,imread(S1(m-low+1,:)));
    end
end
end

%% remove blank front array
C(:,:,1)=[];
D(:,:,1)=[];
r(:,:,1)=[];
q(:,:,1)=[];
if normalization==1
H(:,:,1)=[];
I(:,:,1)=[];
end

%% remove background
C(:,:,1:N)=double(C(:,:,1:N))-double(r(:,:,1:N));
D(:,:,1:N)=double(D(:,:,1:N))-double(q(:,:,1:N));
if normalization==1
H(:,:,1:N)=double(H(:,:,1:N))-double(r(:,:,1:N));
I(:,:,1:N)=double(I(:,:,1:N))-double(q(:,:,1:N));
end


%% Image Translation
up=220;
over=105;
up1=220;%220, 105
over1=105;

E(:,:,:)=imtranslate(D(:,:,:),[over,-up]);
F(:,:,:)=E(1:(1080-up),(1+over):1920,:);
G(:,:,:)=C(1:(1080-up),(1+over):1920,:);

if normalization ==1
K(:,:,:)=imtranslate(I(:,:,:),[over1,-up1]);
J(:,:,:)=H(1:(1080-up1),(1+over1):1920,:);
M(:,:,:)=K(1:(1080-up1),(1+over1):1920,:);
end
%% Damping Out Banding
for a=1:N
    for b=2:(1920-over-1)
     for z=2:(1080-up-1)
         G(z,b,a)=mean(mean(G(z-1:z+1,b-1:b+1,a)));
     end
    end
    for b=1:(1920-over)
        G(1,b,a)=mean(mean(G(1:2,b,a)));
        G(1080-up,b,a)=mean(mean(G(1080-up-1:1080-up,b,a)));
    end
    for z=1:(1080-up)
        G(z,1,a)=mean(mean(G(z,1:2,a)));
        G(z,1920-over,a)=mean(mean(G(z,1920-over-1:1920-over,a)));
    end
```

```
end
if normalization ==1
for a=1:N
    for b=2:(1920-over-1)
     for z=2:(1080-up-1)
         J(z,b,a)=mean(mean(J(z-1:z+1,b-1:b+1,a)));
     end
    end
    for b=1:(1920-over)
        J(1,b,a)=mean(mean(J(1:2,b,a)));
        J(1080-up,b,a)=mean(mean(J(1080-up-1:1080-up,b,a)));
    end
    for z=1:(1080-up)
        J(z,1,a)=mean(mean(J(z,1:2,a)));
        J(z,1920-over,a)=mean(mean(J(z,1920-over-1:1920-over,a)));
    end
end
end
%% Correct for path length and Cross over
top=zeros(50,N);
count=0;
Gcorrected(:,:,:)=G(:,:,:)./exp(-psi*PL);
Fcorrected=double(F)-double(G).*onetenratio;

%% Image Normalization
if normalization==1
M(:,:,:)=double(M(:,:,:))-double(J(:,:,:)).*onetenratio1;
J(:,:,:)=double(J(:,:,:))./exp(-psi*PL1);

Gnormalized=zeros(1080-up,1920-over,N);
Fnormalized=zeros(1080-up,1920-over,N);
O=double(zeros(1080-up1,1920-over1,N));
P=double(zeros(1080-up1,1920-over1,N));

for a=1:N
    O(:,:,1)=O(:,:,1)+double(J(:,:,a));
    P(:,:,1)=P(:,:,1)+double(M(:,:,a));
end
O(:,:,1)=O(:,:,1)/N;
P(:,:,1)=P(:,:,1)/N;

for a=1:N
Gnormalized(:,:,a)=double(Gcorrected(:,:,a))./double(O(:,:,1));
Fnormalized(:,:,a)=double(Fcorrected(:,:,a))./double(P(:,:,1));
end
end

%%Determine temperature

if normalization==1
    tempratio=Fnormalized./double(Gnormalized);
else
    tempratio=Fcorrected./double(Gcorrected);
end
```

```
temperature=zeros(size(tempratio));
temperature(:,:,:)=double((B-tempratio(:,:,:))./(A));

%% temperature image local Average, Std, High, Low
averagetemp=zeros(N,1);
stdtemp=zeros(N,1);
hightemp=zeros(N,1);
lowtemp=zeros(N,1);
for a=1:N
averagetemp(a,1)=mean(mean(temperature(:,:,a)));
stdtemp(a,1)=std2(temperature(:,:,a));
hightemp(a,1)=max(max(temperature(:,:,a)));
lowtemp(a,1)=min(min(temperature(:,:,a)));
end
disp(averagetemp);
disp(stdtemp);

%% Exporting summary of local temperature data

summarytemp=zeros(N,3);
summarytemp(:,1)=averagetemp(:,1);
summarytemp(:,2)=stdtemp(:,1);
summarytemp(:,3)=hightemp(:,1);
summarytemp(:,4)=lowtemp(:,1);
filename='C:\Users\Student\Desktop\Temperature';
xlswrite(filename,summarytemp);


%% Colormap of Temperature Plot

figure, image(temperature(:,:,24)');%Invert to get top of tank on top and
left of tank to be left of image

h5=colorbar; set(h5,'ylim',[15 35]);
colormap(hsv(50));
```